in a hospital with highly prevalent fluoroquinolone resistance. Leuk Lymphoma 52: 131–3.
23. Bow EJ. (2011) Fluoroquinolones, antimicrobial resistance and neutropenic cancer patients. Curr Opin Infect Dis 24: 545–53.
24. Oteo J, Perez-Vazquez M, Campos J. (2010) Extended-spectrum [beta]-lactamase producing Escherichia coli: changing epidemiology and clinical impact. Curr Opin Infect Dis 23: 320–6.
25. Chong Y, Shimoda S, Yakushiji H, Ito Y, Miyamoto T, et al. (2013) Community spread of extended-spectrum beta-lactamase-producing Escherichia coli, Klebsiella pneumoniae and Proteus mirabilis: a long-term study in Japan. J Med Microbiol 62: 1038–43.

Cancer Science
Japanese Cancer Association JCA
Open Access

Nuclear export signal within CALM is necessary for CALM-AF10-induced leukemia

Mai Suzuki,[1] Kazutsune Yamagata,[1] Mika Shino,[1] Yukiko Aikawa,[1] Koichi Akashi,[2] Toshio Watanabe[3] and Issay Kitabayashi[1]

[1]Division of Hematological Malignancy, National Cancer Center Research Institute, Tokyo; [2]Department of Medicine and Biosystemic Science, Kyushu University Graduate School of Medical Science, Fukuoka; [3]Department of Biological Science, Graduate School of Humanities and Sciences, Nara Women's University, Nara, Japan

Key words
AF10, chromosome translocation, histone modification, leukemia, nuclear export signal

Correspondence
Issay Kitabayashi, Division of Hematological Malignancy, National Cancer Center Research Institute, Tsukiji 5-1-1, Chuo-ku, Tokyo 104-0045, Japan.
Tel: +81-3-3542-2511; Fax: +81-3542-0688;
E-mail: ikitabay@ncc.go.jp

Funding Information
Ministry of Health, Labor, and Welfare. Ministry of Education, Culture, Sports, Science, and Technology. National Cancer Center Research and Development Fund. Naito Foundation. Cosmetology Research Foundation. Nara Women's University Intramural Grant for Project Research.

Received September 16, 2013; Revised December 5, 2013; Accepted December 30, 2013

Cancer Sci **105** (2014) 315–323

doi: 10.1111/cas.12347

The *CALM–AF10* fusion gene, which results from a t(10;11) translocation, is found in a variety of hematopoietic malignancies. Certain *HOXA* cluster genes and *MEIS1* genes are upregulated in patients and mouse models that express CALM-AF10. Wild-type clathrin assembly lymphoid myeloid leukemia protein (CALM) primarily localizes in a diffuse pattern within the cytoplasm, whereas AF10 localizes in the nucleus; however, it is not clear where CALM-AF10 acts to induce leukemia. To investigate the influence of localization on leukemogenesis involving CALM-AF10, we determined the nuclear export signal (NES) within CALM that is necessary and sufficient for cytoplasmic localization of CALM-AF10. Mutations in the NES eliminated the capacity of CALM-AF10 to immortalize murine bone-marrow cells *in vitro* and to promote development of acute myeloid leukemia in mouse models. Furthermore, a fusion of AF10 with the minimal NES can immortalize bone-marrow cells and induce leukemia in mice. These results suggest that during leukemogenesis, CALM-AF10 plays its critical roles in the cytoplasm.

The chromosome translocation t(10;11)(p13;q14), found in T-cell acute lymphoblastic leukemia (T-ALL), acute myeloid leukemia (AML) and malignant lymphomas, results in the fusion of the clathrin assembly lymphoid myeloid leukemia protein (*CALM*) and *AF10* [1,2]. The CALM–AF10 fusion protein consists of almost all CALM and AF10 proteins, with the exception of one or two plant homeodomain (PHD).[1,3] AF10, also known as MLLT10, interacts with the transcription factor Ikaros and H3K4me3 through its octapeptide motif–leucine zipper (OM-LZ) region and PHD domains, respectively.[4–6] In both mice and humans, CALM-AF10 upregulates certain *HOXA* cluster genes (*HOXA5*, *HOXA7*, *HOXA9* and *HOXA10*) and *MEIS1*.[7,8] *Hoxa5* upregulation, which is critical for CALM-AF10-induced leukemogenesis,[9,10] is mediated by an interaction between the AF10 OM-LZ region and the histone methyltransferase DOT1L, resulting in H3K79 hypermethylation at the *Hoxa5* locus.[9] These findings suggest that CALM-AF10 might function in the nucleus.

The CALM protein shuttles between the cytoplasm and the nucleus under the control of a CRM1-dependent nuclear export signal (NES).[11] In contrast to AF10, which localizes in the nucleus,[4] CALM-AF10 primarily localizes in the cytoplasm.[6,9] Other fusion partners of AF10 in acute myeloid and lymphoid leukemias include MLL, DDX3 and HNRNPH1.[12,13] MLL and hnRNPH1 primarily localize in the nucleus,[14,15] whereas DDX3, like CALM, is mostly distributed throughout the cytoplasm.[16,17] These observations prompted us to investigate whether CALM-AF10 exerts its function in the nucleus or the cytoplasm. We found that mutant CALM-AF10 lacking the NES localized in the nucleus and lost its ability to induce leukemia in mice. Conversely, a fusion consisting of the minimal NES and AF10 localized in the cytoplasm and induced leukemia. These results indicate that the cytoplasmic location of CALM-AF10 is critical for its role in leukemogenesis.

Materials and Methods

Generation of *CALM-AF10* mutant constructs. Plasmid encoding pcDNA3β-FLAG-CALM-AF10 was a gift from Y. Zhang (Department of Biochemistry and Biophysics, University of North Carolina).[9] Plasmid encoding the NES-deficient mutant FLAG-CALM^{NES4A}-AF10 and FLAG-CALM^{NES4A} were generated by introducing four point mutations into the CALM NES sequence by inverse PCR using a site-specific mutagenesis kit (Toyobo, Osaka, Japan).[18] Specifically, leucine (L)-544, L-547, L-551 and isoleucine (I)-553 in the putative NES sequence within CALM-AF10 were replaced by alanine (A), using the following primers: L544A, 5′-GCAGCCAACCTTGTGG

GCAATCTTGGC-3′, and 5′-AGATGAATCCAAGTCATCAGA TACT-3′; L547A, 5′-GCTGTGGGCAATCTTGGCATCGGAA AT-3′, and 5-′GTTGGCTGCAGATGAATCCAAGTCA-3′; L551A, 5′-GCTGGCATCGGAAATGGAACCACTAAG-3′, and 5′-ATT GCCCACAGCGTTGGCTGCAGAT-3′; I553A, 5′-GCCGGAAA TGGAACCACTAAGAATGAT-3′, and 5′-GCCAGCATTGCCC ACAGCGTTGGCT-3′. All mutations were confirmed by DNA sequencing. The AF10 sequence encoding amino acids 81–1027 (mAF10) was amplified by PCR and cloned into pcDNA3β-FLAG. To generate the fusion of the minimal NES with AF10, NES1 (amino acids 543–554) or NES2 (amino acids 539–558) within CALM was generated by PCR amplification using FLAG-CALM-AF10 as a template, and then cloned into pcDNA3β-FLAG-mAF10. The pMY-IG-FLAG-CALM-AF10-IRES-GFP, pMY-IG-FLAG-CALM^{NES4A}-AF10-IRES-GFP, pMY-IG-FLAG-mAF10-IRES-GFP and pMY-IG-FLAG-NES2-AF10-IRES-GFP constructs were generated by inserting the corresponding cDNA into the pMY-IG/IRES-GFP vector.

Cell culture and transfection. COS-7 cells were maintained in DMEM supplemented with 10% FBS, 100 U/mL penicillin, 100 μg/mL streptomycin and 2 mM L-glutamine at 37°C in a humidified 5% CO_2 incubator. COS-7 cells were transfected with pcDNA3β-FLAG constructs using the Effectene Transfection Reagent (Qiagen, Hilden, Germany).

Immunofluorescence analysis. Forty-eight hours after transfection, COS-7 cells transfected with pcDNA3β-FLAG constructs were fixed with 3.7% formaldehyde in PBS and examined by immunofluorescence staining with anti-FLAG M2 monoclonal antibody (Sigma-Aldrich, St. Louis, MO, USA), followed by secondary Alexa Fluor 488-conjugated goat anti-mouse IgG (Invitrogen, Carlsbad, CA, USA). Stained cells were mounted in VECTASHIELD mounting medium and observed using a BX50 fluorescence microscope (Olympus, Tokyo, Japan). Cytospins of murine bone-marrow cells transduced with pMY-IG/IRES-GFP viral constructs encoding FLAG-CALM-AF10, FLAG-CALM^{NES4A}-AF10, FLAG-NES2-AF10 or FLAG-mAF10 were fixed with 4% paraformaldehyde and stained with anti-FLAG M2 monoclonal antibody (Sigma-Aldrich) and anti-KMT4/DOT1L polyclonal rabbit antibody (Abcam, Cambridge, MA, USA), followed by secondary Alexa Fluor 568-conjugated goat anti-mouse IgG (Invitrogen) and Alexa Fluor 488-conjugated goat anti-rabbit IgG (Invitrogen), respectively. Stained bone-marrow cells were mounted in VECTASHIELD mounting medium with DAPI (Vector Laboratories, Burlingame, CA, USA) or Prolong Gold (Invitrogen) and observed under a BZ-9000 fluorescence microscope (Keyence Corporation, Osaka, Japan) or a FluoView FV10i confocal laser scanning microscopy (Olympus).

Retroviral infection and bone-marrow transplantation. C57BL/6J mice were purchased from CLEA Japan (Tokyo, Japan). All mouse experiments were approved by the National Cancer Center Animal Ethics Committee and performed in accordance with the institutional guidelines. The pMY-IG/IRES-GFP constructs encoding FLAG-CALM-AF10, FLAG-CALM^{NES4A}-AF10, FLAG-NES2-AF10 or FLAG-mAF10 were transfected into PLAT-E cells using the GeneJuice transfection reagent (Novagen, Nottingham, UK), and retrovirus supernatants were collected 48 h after transfection. c-kit$^+$ cells (1×10^5 cells), selected from murine total bone-marrow cells using CD117 MicroBeads (Miltenyi Biotec, Bergisch Gladbach, Germany), were incubated with the retrovirus and RetroNectin (Takara Bio, Madison, WI, USA) for 24 h in StemPro-34 SFM medium (Invitrogen) containing cytokines (20 ng/mL SCF, 10 ng/mL IL-6 and 10 ng/mL IL-3). The transduced donor bone-marrow cells were then transplanted into lethally irradiated (9.5 Gy) 7–8-week-old female C57BL/6J recipient mice by intravenous injection. For secondary transplants, bone-marrow cells from the primary leukemia mice were intravenously injected into sub-lethally irradiated (6 Gy) female C57BL/6J mice.

Serial-replating assay. Bone-marrow cells transduced with pMY-IG/IRES-GFP constructs encoding FLAG-CALM-AF10, FLAG-CALM^{NES4A}-AF10, FLAG-NES2-AF10 or FLAG-mAF10 were cultured for 3 days in methylcellulose medium (MethoCult M3234; StemCell Technologies, Vancouver, Canada) supplemented with murine SCF, IL-3 and GM-CSF. The GFP$^+$ cells in methylcellulose medium were then sorted using a JSAN cell sorter (Bay Bioscience, Kobe, Japan) and replated every 3–4 days in methylcellulose medium; colonies and cells were counted at each passage. Cells from the second-round and fifth-round colonies were harvested and analyzed by real-time PCR (RT-PCR).

Real time-PCR analysis. Total RNA from replating colonies was purified using an RNeasy Mini Kit (Qiagen). Purified RNA were reverse-transcribed into cDNA using the High Capacity cDNA Reverse Transcription Kit (Applied Biosystems, Foster City, CA, USA). Real-time PCR was performed using the 7500 Fast Real-time PCR System (Applied Biosystems) using the FastStart Universal Probe Master with ROX (Roche, Basel, Switzerland) and the following TaqMan probes (Applied Biosystems): *Hoxa5* (Mm04213381_s1), *Hoxa7* (Mm00657963_m1), *Hoxa9* (Mm00439364_m1), *Hoxa10* (Mm00433966_m1) and *Meis1* (Mm00487664_m1). The relative expression levels of these genes were normalized against the level of *Actb* (Mm00607939_s1).

Flow-cytometry analysis. Bone-marrow cells from leukemic mice were pre-incubated with rat IgG (Sigma-Aldrich), and then incubated on ice with the appropriate staining reagents: anti-CD115(CSF1R)-PE (eBioscience, San Diego, CA, USA), anti-Mac-1(M1/70)-PE-Cy7 (eBioscience), anti-Gr-1(RB6-8C5)-APC (BD Pharmingen, San Diego, CA, USA) and anti-c-Kit(2B8)-APC-eF780 (eBioscience). FACS analysis and cell sorting were performed using the JSAN cell sorter and the results were analyzed using the FLOWJO software (Tree Star, Standford, CA, USA).

Results

The nuclear export signal within CALM is required for cytoplasmic localization of CALM-AF10. To investigate the role of subcellular localization of CALM-AF10 in leukemogenesis, we focused on the NES within the CALM portion of the fusion protein (amino acids 543–554 of CALM).[9] We generated NES-deficient mutants CALM^{NES4A}-AF10 and CALM^{NES4A}, in which leucine-544, leucine-547, leucine-551 and isoleucine-553 in the putative NES region within CALM were substituted with alanines (NES4A) (Fig. 1a). Expression vectors for FLAG-tagged CALM-AF10, CALM, CALM^{NES4A}-AF10, CALM^{NES4A} and mAF10 (the AF10 portion of CALM-AF10) were transiently transfected into COS-7 cells. Immunofluorescence analysis revealed that CALM and CALM-AF10 primarily localized in the cytoplasm, whereas mAF10 and the NES mutants CALM^{NES4A}-AF10 and CALM^{NES4A} localized in the nucleus (Fig. 1b,c).

To determine the minimal NES, two sequences, NES1 (aa. 543–554) and NES2 (aa. 539–558), were fused to AF10 (Fig. 1a,b). As with mAF10, NES1-AF10 was in the nucleus; by contrast, NES2-AF10 was in the cytoplasm (Fig. 1d). The same results were obtained when these fusion proteins were transduced into murine hematopoietic progenitor cells by retro-

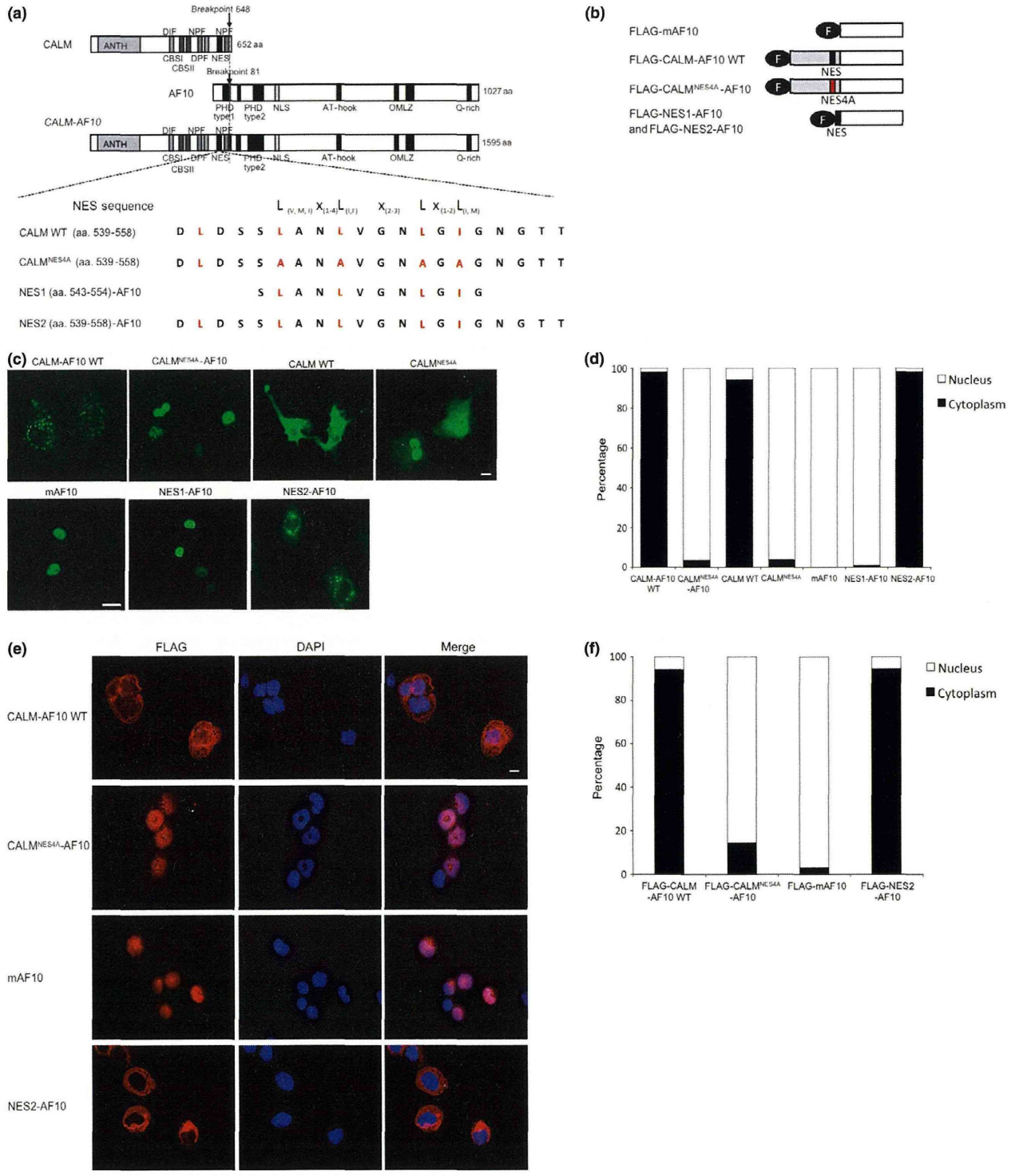

Fig. 1. The NES region within clathrin assembly lymphoid myeloid leukemia protein (CALM) is necessary for cytoplasmic localization. (a) Schematic representations of CALM, AF10, CALM-AF10 and mutant proteins. FLAG-CALM^{NES4A}-AF10 and FLAG-CALM^{NES4A} were generated by alanine substitution of three leucine residues and one isoleucine residue in the putative CALM NES (red). FLAG-NES1-AF10 and FLAG-NES2-AF10 mutants were constructed by fusion of the NES sequences of CALM to the AF10 portion of CALM-AF10. (b) Diagrams of the plasmid constructs used in transfection experiments. (c) Subcellular distribution of CALM-AF10 and the NES point mutations FLAG-CALM-AF10, FLAG-CALM, FLAG-CALM^{NES4A}-AF10, FLAG-CALM^{NES4A}, and FLAG-NES1-AF10, FLAG-NES2-AF10 and FLAG-mAF10 in COS-7 cells. Transfected cells were stained with anti-FLAG antibody (green) and observed by fluorescence microscopy. (d) Population of cells expressing transduced genes in the nucleus and cytoplasm shown in (c). (e) Subcellular distribution of CALM-AF10 and NES mutation proteins in murine bone-marrow cells. Transduced cells were stained with anti-FLAG antibody (red). (f) Population of cells expressing transduced genes in the nucleus and the cytoplasm shown in (e). Nuclei were stained with DAPI (blue) and observed by fluorescence microscopy. The scale bar represents 20 μm in (c) and 10 μm in (e). ANTH, AP180 N-terminal homology domain binding phosphatidylinositol 4,5-bisphosphate (PIP_2); DIF and DPF, motifs interacts with AP-2; NPF, a motif interacts with the EH (Eps15 homology) domain; CBS-I and -II, putative type I and II clathrin-binding sequences; NES, nuclear export signal; PHD Type1 and 2, plant homeodomain zinc finger domains; NLS, nuclear localization signal; AT-hook, DNA-binding protein motif; OMLZ, octapeptide motif-leucine zipper domain; Q-rich, glutamine-rich region.

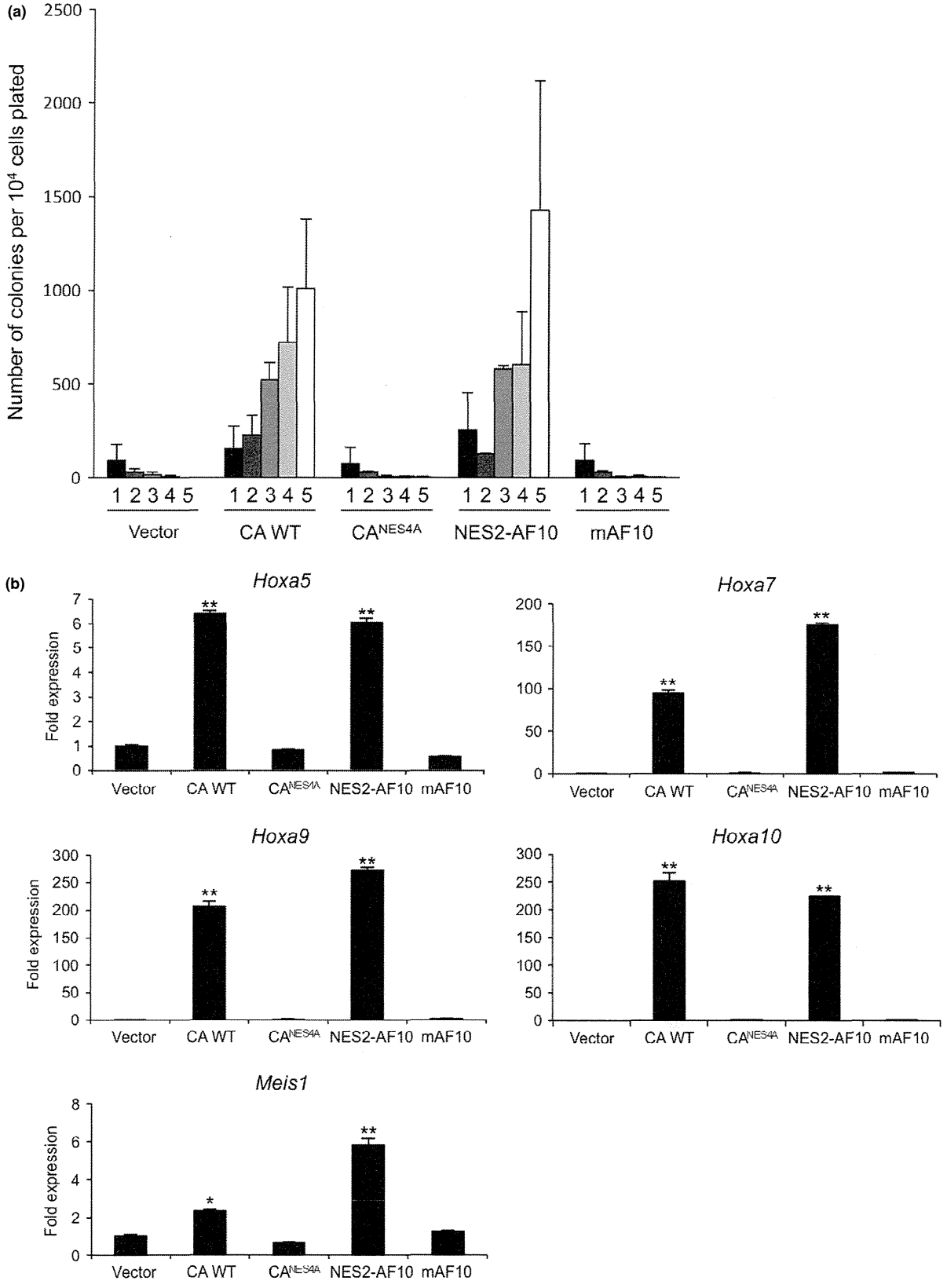

Fig. 2. The nuclear export signal within clathrin assembly lymphoid myeloid leukemia protein (CALM) is critical for *in vitro* immortalization of cells by CALM-AF10. (a) Serial colony-replating assays of murine bone-marrow cells transduced with FLAG-tagged wild-type and mutant CALM-AF10. In each round of replating, 3×10^4 transduced bone-marrow cells were plated. Bars represent the numbers of colonies. (b) *Hoxa* cluster and *Meis1* expression in cells transduced with wild-type or mutant CALM-AF10. RNA transcripts were analyzed by real-time PCR of murine bone-marrow cells transduced with wild-type and mutant CALM-AF10 *in vitro*. Expression levels of *Hoxa5*, *Hoxa7*, *Hoxa9*, *Hoxa10* and *Meis1* were normalized against *Actb* expression and compared with the levels in vector-transfected whole bone-marrow cells. Data are shown as means ± SEM from three independent samples. $*P < 0.05$; $**P < 0.01$. (*vs* normal bone-marrow cells). CA WT, wild-type CALM-AF10.

viral infection (Fig. 1e). These results indicate that NES1 is not sufficient, but its flanking regions including leucine-540 are necessary for cytoplasmic localization of CALM-AF10. Thus, we concluded that the NES2 region is the minimal NES that mediates cytoplasmic localization of CALM-AF10.

The nuclear export signal within CALM is necessary for CALM-AF10-induced immortalization of cells *in vitro*. We next investigated whether the NES within CALM-AF10 is required for leukemogenesis. To this end, primary murine bone-marrow stem/progenitor cells (HSPC) were infected with retrovirus encoding CALM-AF10, CALM^{NES4A}-AF10, NES2-AF10 and mAF10. Serial-replating assays revealed that both CALM-AF10 and NES2-AF10 immortalized HSPC, and that the cells formed colonies for at least five rounds of replating (Fig. 2a). By contrast, neither mAF10 nor CALM^{NES4A}-AF10, which lacks a functional CALM NES, could immortalize cells. Transduced cells with elevated colony-forming abilities also exhibited upregulation of the *Hoxa* cluster (*Hoxa5*, *Hoxa7*, *Hoxa9* and *Hoxa10*) and *Meis1* genes (Fig. 2b)[7,9]. These results indicated that the CALM NES is necessary for CALM-AF10 to immortalize hematopoietic stem/progenitor cells.

The nuclear export signal within CALM-AF10 is necessary to induce leukemia *in vivo*. To determine whether CALM-AF10 and NES2-AF10 can induce leukemia in mice, we injected bone-marrow progenitor cells transduced with CALM-AF10 and NES2-AF10 into lethally irradiated mice. Seven out of eight mice transplanted with cells expressing CALM-AF10 developed leukemia within 6 months after transplantation (Fig. 3a), and all mice transplanted with cells expressing NES2-AF10 developed leukemia within 3 months after transplantation. When cells prepared from bone marrow of these leukemic mice were transplanted into secondary recipient mice, all recipients promptly developed leukemia (medians: CALM-AF10 donors, 21 days [n = 4]; NES2-AF10 donors,

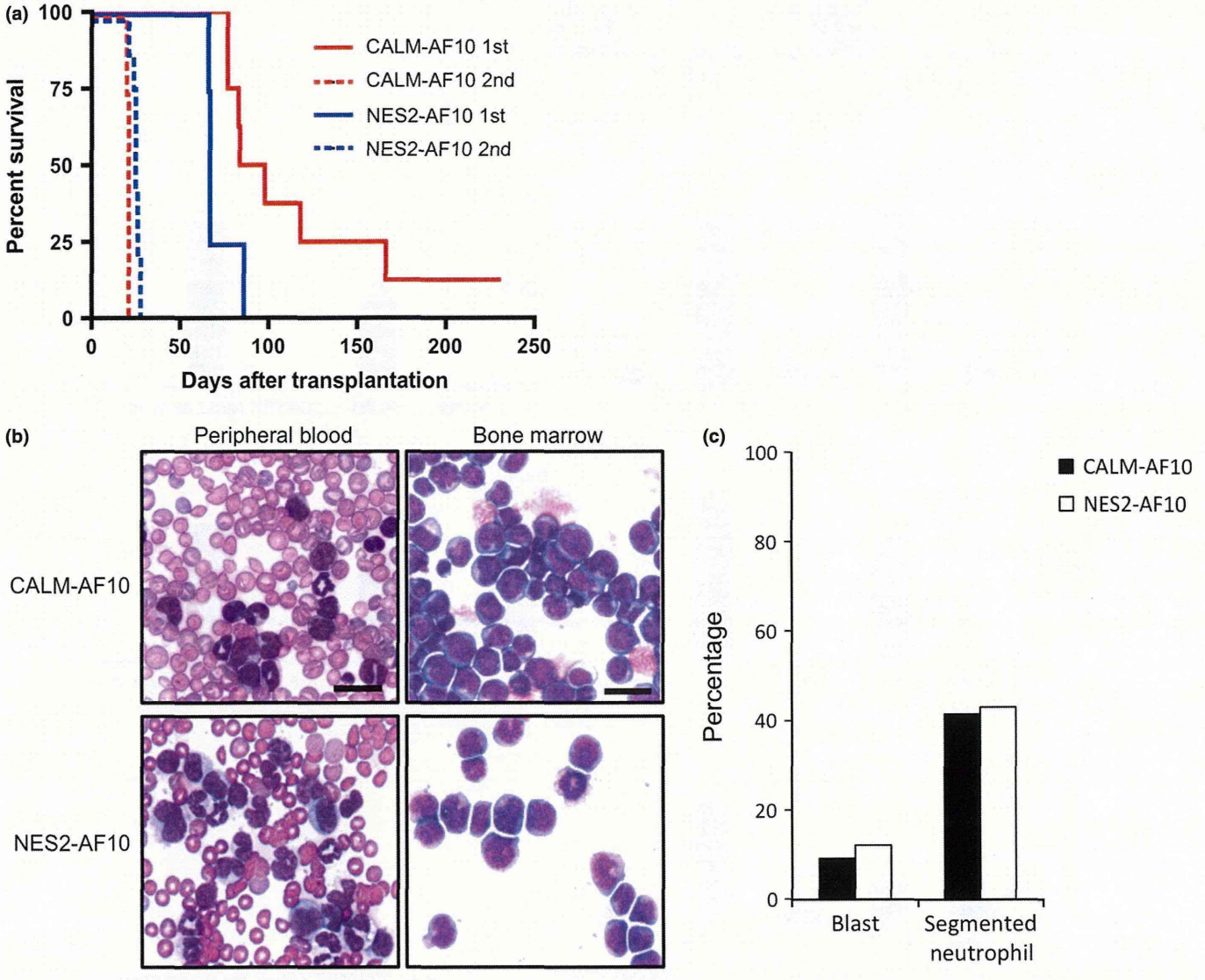

Fig. 3. The nuclear export signal within clathrin assembly lymphoid myeloid leukemia protein (CALM) is sufficient for leukemic transformation by CALM-AF10. (a) Survival of mice injected with murine bone-marrow cells transduced with FLAG-CALM-AF10 or FLAG-NES2-AF10. The leukemia-free survivals of the mice were analyzed. CALM-AF10 primary transplantation, n = 8; CALM-AF10 secondary transplantation, n = 4; NES2-AF10 primary transplantation, n = 4; NES2-AF10 secondary transplantation, n = 9. (b) Peripheral blood smears and bone-marrow cytospins were stained with May-Giemsa from CALM-AF10-transduced or NES2-AF10-transduced bone-marrow cells. Original magnification is 400×. (c) Population of blasts and segmented neutrophils in bone-marrow cells shown in (b). The scale bars represent 20 μm.

25 days [n = 9]). Morphological analysis revealed large populations of blast cells in leukemic mice receiving cells transduced with either CALM-AF10 or NES2-AF10 (Fig. 3b, c). Flow cytometry analysis showed that cells expressing CALM-AF10 and NES2-AF10 in the bone marrow cells of primary recipient mice were Mac1$^+$, CSF1R$^+$ and c-kit$^+$ (Fig. 4a). Moreover, as shown in Figure 4b, *Hoxa5*, *Hoxa7*, *Hoxa9*, *Hoxa10* and *Meis1* expression levels were upregulated in cells expressing CALM-AF10 and NES2-AF10 compared with normal bone marrow cells, although upregulation of *Hoxa5* and *Meis1* in primary recipient mice harboring NES2-AF10 was not significant (P = 0.084 and P = 0.093, respectively). These

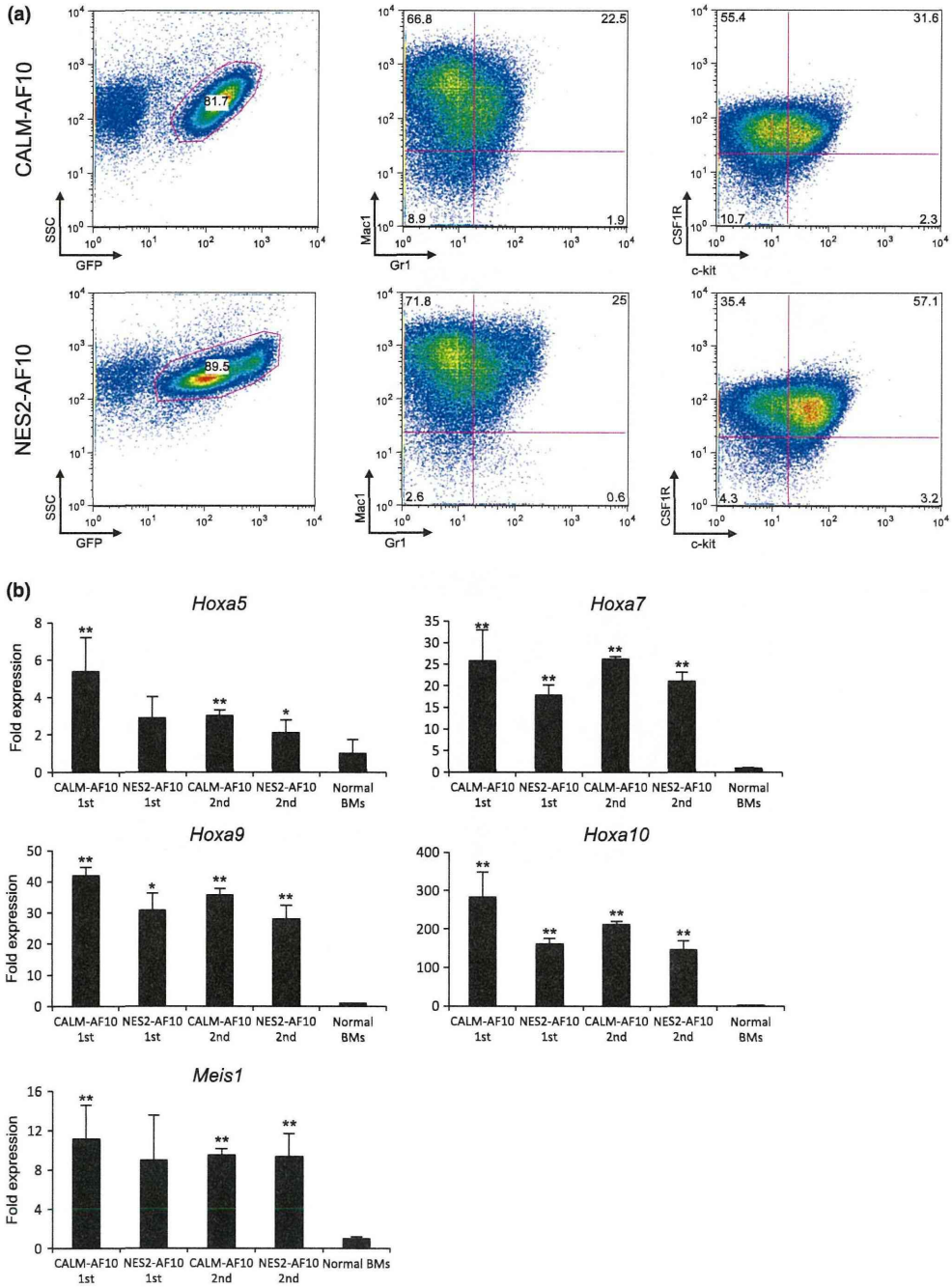

Fig. 4. Characterization of leukemic cells *in vivo*. (a) Flow cytometric analysis of leukemic cells. Murine bone-marrow cells were prepared from mice that developed leukemia after receiving transplantation of tumor cells transduced with CALM-AF10 or NES2-AF10, and were co-stained for Gr-1, Mac-1, colony stimulating factor 1 receptor (CSF1R) and c-kit; data are representative of CALM-AF10 primary transplantation (n = 3) and NES2-AF10 primary transplantation (n = 3). (b) *Hoxa* cluster and *Meis1* expression in mice receiving cells transduced with wild-type and mutant CALM-AF10. RNA transcripts were analyzed by real-time PCR of bone-marrow cells in mice that developed leukemia after CALM-AF10 and NES2-AF10 bone-marrow transplantation. Expression levels of *Hoxa5*, *Hoxa7*, *Hoxa9*, *Hoxa10* and *Meis1* were normalized against *Actb* and compared with wild-type whole bone marrow. Data are shown as means ± SEM from three independent leukemic mice. *P < 0.05; **P < 0.01 (*vs* normal bone-marrow cells).

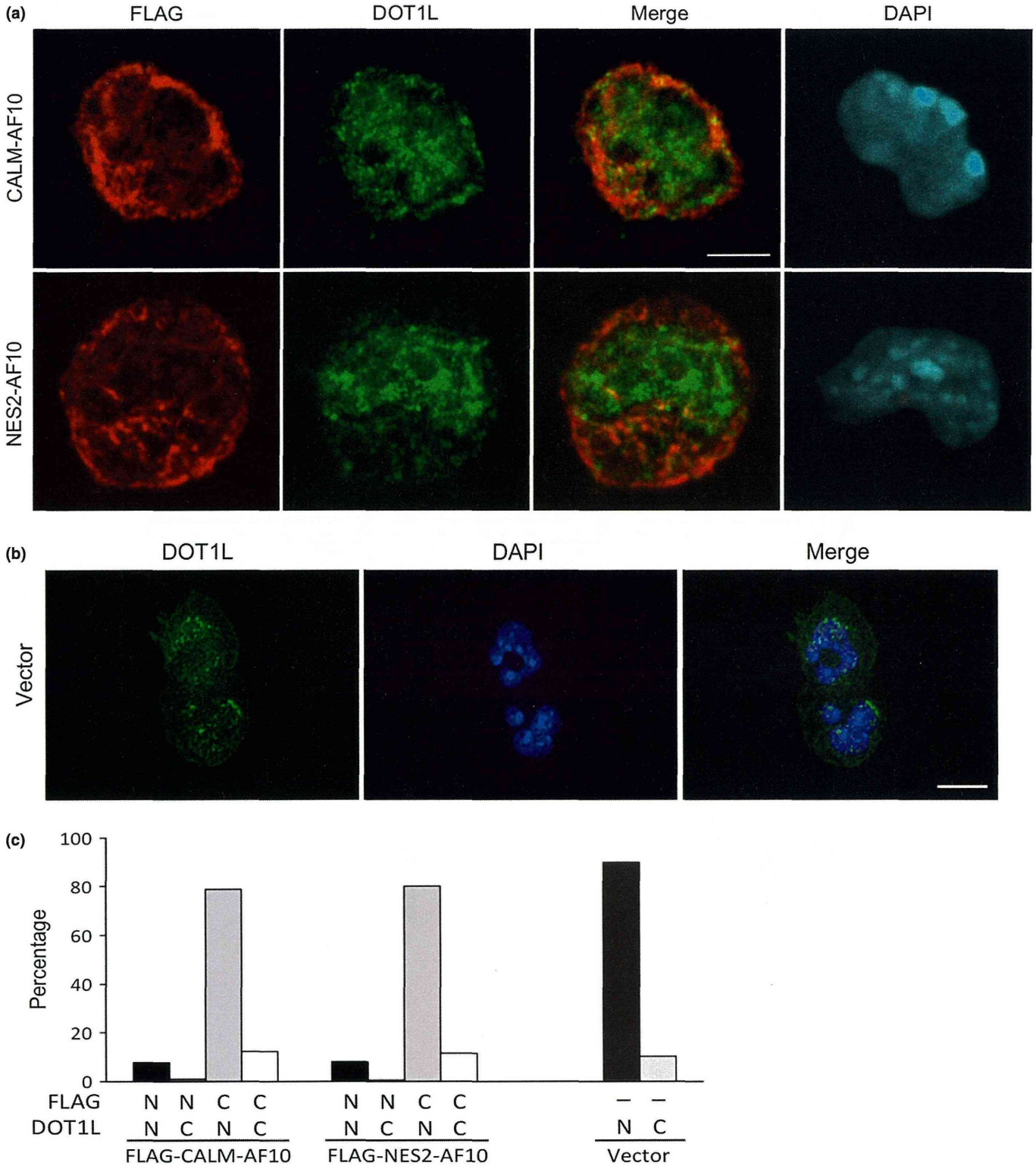

Fig. 5. Dot1L mainly localize in the nucleus in CALM-AF10-induced or NES2-AF10-induced leukemic cells. (a) Subcellular distribution of endogenous Dot1L in CALM-AF10-induced or NES2-AF10-induced leukemic cells. Cytospins of the cells were stained with anti-FLAG antibody (red), anti-DOT1L antibody (green) and DAPI (blue) and observed by confocal laser scanning microscopy. Note that GFP expression was not detected in the condition. (b) Subcellular distribution of endogenous Dot1L in the control vector-infected murine using fluorescence microscopy. (c) Population of leukemia cells expressing DOT1L and CALM-AF10 or FLAG-NES2-AF10 in the nucleus and the cytoplasm shown in (a) and (b). The scale bar represents 5 μm in (a) and 10 μm in (b).

data demonstrate that the NES within CALM-AF10 is a critical element for induction of leukemia.

It has been reported that CALM-AF10 interacts with the histone methyltransferase DOT1L to mediate H3K79 hypermethylation at the *Hoxa5* locus.[9] To determine whether Dot1L colocalizes with CALM-AF10 and NES2-AF10 in the leukemia cells, we performed immunofluorescence analysis. Dot1L mainly localized in the nucleus while CALM-AF10 and NES2-AF10 mainly localized in the cytoplasm (Fig. 5a,b). Dot1L partially colocalized with both CALM-AF10 and NES2-AF10, but neither CALM-AF10 nor NES2-AF10 altered the localization of Dot1L (Fig. 5a).

Discussion

AF10 and CALM localize diffusely in the nucleus and cytoplasm, respectively, whereas CALM-AF10 primarily localizes in cytoplasmic speckle domains (see Fig. 1c,d). The fact that CALM-AF10 regulates histone methylation at the *Hoxa5* locus suggests that CALM-AF10 is likely to function in the nucleus.[9] However, the results described here indicate that the CALM NES is essential for CALM-AF10-induced leukemogenesis, suggesting that cytoplasmic localization (or shuttling between nucleus and cytoplasm) is critical for the function of CALM-AF10. During the preparation of the manuscript, another group reported similar findings,[19] indicating that the results are reproducible and the conclusions can be validated using alternative experimental systems.

The molecular mechanism by which CALM-AF10 exerts its function in the cytoplasm remains unclear, but two possibilities are consistent with the existing data: CALM-AF10 may affect cytoplasmic signaling pathways that regulate expression of its target genes, including *HoxA* cluster genes; alternatively, CALM-AF10 may affect the functions of transcriptional regulators by changing their localization from the nucleus to the cytoplasm. DOT1L, a candidate mediator of CALM-AF10-induced leukemia, interacts with AF10 and induces H3K79 hypermethylation at *Hoxa5*.[9] However, our present data suggest that CALM-AF10 and NES2-AF10 did not affect the localization of Dot1L (see Fig. 5a). It is possible that CALM-AF10 squelches DOT1L inhibitors by exporting them to the cytoplasm.

CALM plays an important role in clathrin-mediated endocytosis.[17,20,21] It and other endocytosis-related genes, such as EPS15, EEN, CLTC and HIP1, are involved in multiple types of leukemia-associated chromosomal translocations (e.g. MLL-CALM, MLL-EPS15, MLL-EEN, CLTC-ALK and HIP1-PDGFBR),[22–26] suggesting that these leukemia-associated fusions might affect endocytosis in a manner that contributes to leukemogenesis. However, recent reports have shown that the clathrin-binding domain of CALM is not essential for CALM-AF10-mediated leukemogenesis.[27,28] Here, we show that nuclear export of CAL-AF10 is critical for the leukemogenesis. Because the endocytosis-related proteins mentioned above are also exported from the nucleus to the cytoplasm, as in the case of CALM,[11,23,29] it is possible that changes in the localization of fusions involving endocytosis-related proteins have some shared consequence that is important for leukemogenesis.

Molecular exchange between the nucleus and cytoplasm takes place through nuclear pore complexes (NPC). Fusion proteins containing NUP98 and NUP214, which are components of the NPC, have been found in AML and T-ALL;[30,31] as in cells expressing CALM-AF10, a set of *Hoxa* and *Meis1* genes are upregulated in leukemia cells expressing these NUP98 fusions and NUP214 fusions.[32,33] In addition, the NPC-component fusions interact with CRM1, the major receptor for the nuclear export of protein.[33,34] These observations suggest that alteration of the localization of certain factors by NUP98 fusions and NUP214 fusions might be important for leukemogenesis, and that a common mechanism may underlie leukemias induced by CALM and NUP fusions.

Acknowledgments

We thank Dr Y. Zhang for pcDNA3β-FLAG-CALM-AF10 plasmid. This work was supported in part by Grants-in-Aid for Scientific Research from the Ministry of Health, Labor, and Welfare and from the Ministry of Education, Culture, Sports, Science, and Technology; the National Cancer Center Research and Development Fund; the Naito Foundation; Cosmetology Research Foundation; and Nara Women's University Intramural Grant for Project Research. MS is a Research Fellow for Yong Scientist of Japan Society for the Promotion of Science.

Disclosure Statement

The authors have no conflict of interest.

References

1 Dreyling MH, MartinezCliment JA, Zheng M, Mao J, Rowley JD, Bohlander SK. The t(10;11)(p13;q14) in the U937 cell line results in the fusion of the AF10 gene and CALM, encoding a new member of the AP-3 clathrin assembly protein family. *Proc Natl Acad Sci USA* 1996; **93**: 4804–9.
2 Bohlander SK, Muschinsky V, Schrader K *et al.* Molecular analysis of the CALM/AF10 fusion: identical rearrangements in acute myeloid leukemia, acute lymphoblastic leukemia and malignant lymphoma patients. *Leukemia* 2000; **14**: 93–9.
3 Narita M, Shimizu K, Hayashi Y *et al.* Consistent detection of CALM-AF10 chimaeric transcripts in haematological malignancies with t(10;11)(p13;q14) and identification of novel transcripts. *Br J Haematol* 1999; **105**: 928–37.
4 Linder B, Newman R, Jones LK *et al.* Biochemical analyses of the AF10 protein: the extended LAP/PHD-finger mediates oligomerisation. *J Mol Biol* 2000; **299**: 369–78.
5 Wysocka J, Swigut T, Xiao H *et al.* A PHD finger of NURF couples histone H3 lysine 4 trimethylation with chromatin remodelling. *Nature* 2006; **442**: 86–90.
6 Greif PA, Tizazu B, Krause A, Kremmer E, Bohlander SK. The leukemogenic CALM/AF10 fusion protein alters the subcellular localization of the lymphoid regulator Ikaros. *Oncogene* 2008; **27**: 2886–96.
7 Caudell D, Zhang Z, Chung YJ, Aplan PD. Expression of a CALM-AF10 fusion gene leads to Hoxa cluster overexpression and acute leukemia in transgenic mice. *Cancer Res* 2007; **67**: 8022–31.
8 Mulaw MA, Krause A, Deshpande AJ *et al.* CALM/AF10-positive leukemias show upregulation of genes involved in chromatin assembly and DNA repair processes and of genes adjacent to the breakpoint at 10p12. *Leukemia* 2012; **26**: 1012–9.
9 Okada Y, Jiang Q, Lemieux M, Jeannotte L, Su L, Zhang Y. Leukaemic transformation by CALM-AF10 involves upregulation of Hoxa5 by hDOT1L. *Nat Cell Biol* 2006; **8**: 1017–24.
10 Chen L, Deshpande AJ, Banka D *et al.* Abrogation of MLL-AF10 and CALM-AF10-mediated transformation through genetic inactivation or pharmacological inhibition of the H3K79 methyltransferase Dot1l. *Leukemia* 2013; **27**: 813–22.
11 Vecchi M, Polo S, Poupon V, van de Loo JW, Benmerah A, Di Fiore PP. Nucleocytoplasmic shuttling of endocytic proteins. *J Cell Biol* 2001; **153**: 1511–7.
12 Borkhardt A, Haas OA, Strobl W *et al.* A novel type of Mll/Af10 fusion transcript in a child with acute megakaryocytic leukemia (Aml-M7). *Leukemia* 1995; **9**: 1796–7.
13 Brandimarte L, Pierini V, Di Giacomo D *et al.* New MLLT10 gene recombinations in pediatric T-acute lymphoblastic leukemia. *Blood* 2013; **121**: 5064–7.

14 Lee JW, Liao PC, Young KC *et al.* Identification of hnRNPH1, NF45, and C14orf166 as novel host interacting partners of the mature hepatitis C virus core protein. *J Proteome Res* 2011; **10**: 4522–34.
15 Ennas MG, Sorio C, Greim R *et al.* The human ALL-1/MLL/HRX antigen is predominantly localized in the nucleus of resting and proliferating peripheral blood mononuclear cells. *Cancer Res* 1997; **57**: 2035–41.
16 Yedavalli VSRK, Neuveut C, Chi YH, Kleiman L, Jeang KT. Requirement of DDX3 DEAD box RNA helicase for HIV-1 Rev-RRE export function. *Cell* 2004; **119**: 381–92.
17 Tebar F, Bohlander SK, Sorkin A. Clathrin assembly lymphoid myeloid leukemia (CALM) protein: localization in endocytic-coated pits, interactions with clathrin, and the impact of overexpression on clathrin-mediated traffic. *Mol Biol Cell* 1999; **10**: 2687–702.
18 Takagi M, Nishioka M, Kakihara H *et al.* Characterization of DNA polymerase from *Pyrococcus* sp. strain KOD1 and its application to PCR. *Appl Environ Microbiol* 1997; **63**: 4504–10.
19 Conway AE, Scotland PB, Lavau CP, Wechsler DS. A CALM-derived nuclear export signal is essential for CALM-AF10-mediated leukemogenesis. *Blood* 2013; **121**: 4758–68.
20 Ford MGJ, Pearse BMF, Higgins MK *et al.* Simultaneous binding of PtdIns (4,5)P-2 and clathrin by AP180 in the nucleation of clathrin lattices on membranes. *Science* 2001; **291**: 1051–5.
21 Meyerholz A, Hinrichsen L, Groos S, Esk PC, Brandes G, Ungewickell EJ. Effect of clathrin assembly lymphoid myeloid leukemia protein depletion on clathrin coat formation. *Traffic* 2005; **6**: 1225–34.
22 Bernard OA, Mauchauffe M, Mecucci C, Vandenberghe H, Berger R. A novel gene, Af-1p, fused to Hrx in T(1,11)(P32, Q23), is not related to Af-4, Af-9 nor Enl. *Oncogene* 1994; **9**: 1039–45.
23 So CW, So CKC, Cheung N, Chew SL, Sham MH, Chan LC. The interaction between EEN and Abi-1, two MLL fusion partners, and synaptojanin and dynamin: implications for leukaemogenesis. *Leukemia* 2000; **14**: 594–601.
24 Bridge JA, Kanamori M, Ma ZG *et al.* Fusion of the ALK gene to the clathrin heavy chain gene, CLTC, in inflammatory myofibroblastic tumor. *Am J Pathol* 2001; **159**: 411–5.
25 Wechsler DS, Engstrom LD, Alexander BM, Motto DG, Roulston D. A novel chromosomal inversion at 11q23 in infant acute myeloid leukemia fuses MLL to CALM, a gene that encodes a clathrin assembly protein. *Genes Chromosom Cancer* 2003; **36**: 26–36.
26 Ross TS, Bernard OA, Berger R, Gilliland DG. Fusion of Huntingtin interacting protein 1 to platelet-derived growth factor beta receptor (PDGF beta R) in chronic myelomonocytic leukemia with t(5;7)(q33;q11.2). *Blood* 1998; **91**: 4419–26.
27 Deshpande AJ, Rouhi A, Lin Y *et al.* The clathrin-binding domain of CALM and the OM-LZ domain of AF10 are sufficient to induce acute myeloid leukemia in mice. *Leukemia* 2011; **25**: 1718–27.
28 Stoddart A, Tennant TR, Fernald AA, Anastasi J, Brodsky FM, Le Beau MM. The clathrin-binding domain of CALM-AF10 alters the phenotype of myeloid neoplasms in mice. *Oncogene* 2012; **31**: 494–506.
29 Engqvist-Goldstein AEY, Kessels MM, Chopra VS, Hayden MR, Drubin DG. An actin-binding protein of the Sla2/Huntingtin interacting protein 1 family is a novel component of clathrin-coated pits and vesicles. *J Cell Biol* 1999; **147**: 1503–18.
30 von Lindern M, Breems D, van Baal S, Adriaansen H, Grosveld G. Characterization of the translocation breakpoint sequences of two DEK-CAN fusion genes present in t(6;9) acute myeloid leukemia and a SET-CAN fusion gene found in a case of acute undifferentiated leukemia. *Genes Chromosom Cancer* 1992; **5**: 227–34.
31 Nakamura T, Largaespada DA, Lee MP *et al.* Fusion of the nucleoporin gene NUP98 to HOXA9 by the chromosome translocation t(7;11)(p15;p15) in human myeloid leukaemia. *Nat Genet* 1996; **12**: 154–8.
32 Nakamura T. NUP98 fusion in human leukemia: dysregulation of the nuclear pore and homeodomain proteins. *Int J Hematol* 2005; **82**: 21–7.
33 Van Vlierberghe P, van Grotel M, Tchinda J *et al.* The recurrent SET-NUP214 fusion as a new HOXA activation mechanism in pediatric T-cell acute lymphoblastic leukemia. *Blood* 2008; **111**: 4668–80.
34 Takeda A, Sarma NJ, Abdul-Nabi AM, Yaseen NR. Inhibition of CRM1-mediated nuclear export of transcription factors by leukemogenic NUP98 fusion proteins. *J Biol Chem* 2010; **285**: 16248–57.

PLOS ONE

Contribution of Bone Marrow-Derived Hematopoietic Stem/Progenitor Cells to the Generation of Donor-Marker$^+$ Cardiomyocytes *In Vivo*

Mitsuhiro Fukata[1]*, Fumihiko Ishikawa[1,2]*, Yuho Najima[2], Takuji Yamauchi[1], Yoriko Saito[2], Katsuto Takenaka[1], Kohta Miyawaki[1], Hideki Shimazu[1], Kazuya Shimoda[3], Takaaki Kanemaru[4], Keiichiro Nakamura[5], Keita Odashiro[1], Koji Nagafuji[6], Mine Harada[1], Koichi Akashi[1,7]

1 Department of Medicine and Biosystemic Science, Kyushu University Graduate School of Medical Science, Fukuoka, Japan, **2** Laboratory for Human Disease Models, RIKEN Research Center for Allergy and Immunology, Yokohama, Japan, **3** Department of Gastroenterology and Hematology, Faculty of Medicine, Miyazaki University, Miyazaki, Japan, **4** Morphology Core, Kyushu University, Fukuoka, Japan, **5** Second Department of Anatomy, Kurume University School of Medicine, Kurume, Japan, **6** Division of Hematology and Oncology, Department of Medicine, Kurume University School of Medicine, Kurume, Japan, **7** Center for Cellular and Molecular Medicine, Kyushu University Hospital, Fukuoka, Japan

Abstract

Background: Definite identification of the cell types and the mechanism relevant to cardiomyogenesis is essential for effective cardiac regenerative medicine. We aimed to identify the cell populations that can generate cardiomyocytes and to clarify whether generation of donor-marker$^+$ cardiomyocytes requires cell fusion between BM-derived cells and recipient cardiomyocytes.

Methodology/Principal Findings: Purified BM stem/progenitor cells from green fluorescence protein (GFP) mice were transplanted into C57BL/6 mice or cyan fluorescence protein (CFP)-transgenic mice. Purified human hematopoietic stem cells (HSCs) from cord blood were transplanted into immune-compromised NOD/SCID/IL2rγ^{null} mice. GFP$^+$ cells in the cardiac tissue were analyzed for the antigenecity of a cardiomyocyte by confocal microscopy following immunofluorescence staining. GFP$^+$ donor-derived cells, GFP$^+$CFP$^+$ fused cells, and CFP$^+$ recipient-derived cells were distinguished by linear unmixing analysis. Hearts of xenogeneic recipients were evaluated for the expression of human cardiomyocyte genes by real-time quantitative polymerase chain reaction. In C57BL/6 recipients, Lin$^{-/low}$CD45$^+$ hematopoietic cells generated greater number of GFP$^+$ cardiomyocytes than Lin$^{-/low}$CD45$^-$ mesenchymal cells (37.0+/−23.9 vs 0.00+/−0.00 GFP$^+$ cardiomyocytes per a recipient, P = 0.0095). The number of transplanted purified HSCs (Lin$^{-/low}$Sca-1$^+$ or Lin$^-$Sca-1$^+$c-Kit$^+$ or CD34$^-$Lin$^-$Sca-1$^+$c-Kit$^+$) showed correlation to the number of GFP$^+$ cardiomyocytes ($P<0.05$ in each cell fraction), and the incidence of GFP$^+$ cardiomyocytes per injected cell dose was greatest in CD34$^-$Lin$^-$Sca-1$^+$c-Kit$^+$ recipients. Of the hematopoietic progenitors, total myeloid progenitors generated greater number of GFP$^+$ cardiomyocytes than common lymphoid progenitors (12.8+/−10.7 vs 0.67+/−1.00 GFP$^+$ cardiomyocytes per a recipient, P = 0.0021). In CFP recipients, all GFP$^+$ cardiomyocytes examined coexpressed CFP. Human troponin C and myosin heavy chain 6 transcripts were detected in the cardiac tissue of some of the xenogeneic recipients.

Conclusions/Significance: Our results indicate that HSCs resulted in the generation of cardiomyocytes via myeloid intermediates by fusion-dependent mechanism. The use of myeloid derivatives as donor cells could potentially allow more effective cell-based therapy for cardiac repair.

Citation: Fukata M, Ishikawa F, Najima Y, Yamauchi T, Saito Y, et al. (2013) Contribution of Bone Marrow-Derived Hematopoietic Stem/Progenitor Cells to the Generation of Donor-Marker$^+$ Cardiomyocytes *In Vivo*. PLoS ONE 8(5): e62506. doi:10.1371/journal.pone.0062506

Editor: Maurizio Pesce, Centro Cardiologico Monzino, Italy

Received July 14, 2011; **Accepted** March 26, 2013; **Published** May 7, 2013

Funding: The authors have no support or funding to report.

Competing Interests: The authors have declared that no competing interests exist.

* E-mail: mfukata-circ@umin.net (MF); f_ishika@rcai.riken.jp (FI)

Introduction

Modification of regenerative capacity in injured heart could be potentially alternative to conventional therapy for treating patients suffering from heart failure [1–7]. Based on the promising results in rodents [3,4], clinical trials of cellular therapy using bone marrow (BM) cells for ischemic heart disease patients have been designed. In many of clinical trials for improving the function of cardiac recovery, some favorable results were obtained following injection of BM mononuclear cells (MNCs) [2,5–7]. However, careful examination needs to be performed in basic research because cell fate and the effects of transplanted cells are not fully unveiled [8].

BM contains heterogeneous cell populations including at least two distinct stem cells, hematopoietic stem cells (HSCs) and mesenchymal stem cells (MSCs) [9], and various progenitors of myeloid and lymphoid lineages. Both HSCs and MSCs have been reported to acquire the phenotype of cardiomyocytes in syngeneic

or xenogeneic recipients [4,10–13]. However, quantitative analysis of regenerative capacity by each stem fraction has not been performed in the identical transplantation setting.

One proposed mechanism for the phenotypic change of BM-derived cells to tissue-specific cells is cell fusion. Since the original report of spontaneous cell fusion between BM cells and embryonic stem cells [14], it has become apparent that not only some BM-derived cells in the heart and other selective tissues are the consequences of cell fusion at least in part [10,12,15], but also fused BM-derived cells can be reprogrammed to express tissue specific genes [16,17]. On the other hand, BM cells have been reported to generate non-hematopoietic cells in certain tissues without fusion requirement [18,19] although cell fate conversion from HSCs themselves directly to cardiomyocytes has questioned in several studies [10,20,21].

To improve the efficiency of cardiac functional restoration and to minimize adverse effects of cell-based therapy using BM cells, the cell type with the greatest contribution to cardiomyogenesis and mechanisms underlying altered cardiac function need to be clarified *in vivo*. In this study, we examined cardiomyogenic potential of BM cells following syngeneic BM transplantation to identify the cell population in BM that possesses cardiomyogenic potential and to clarify whether cardiomyogenesis by BM-derived cells require cell fusion with recipient cardiomyocytes. Furthermore, we adopted xenogeneic transplantation system to unveil genetic sequences of donor-derived cardiomyocytes through discrimination of the donor gene from the recipient gene. To fully exploit the capacity of stem cells, we employed newborns as recipients, in which age-related decline of regenerative capacity can be restored by environmental factors [22].

Results

Determination of Cell Fate in Cardiac Tissue of Recipient Mice Transplanted with Syngeneic BM Cells

We first created an *in vivo* model for evaluating cell fate of BM cells in cardiac tissue by injecting 10^7 unfractionated green fluorescence protein (GFP) mouse BM cells into irradiated newborn C57BL/6 mice, followed by ventricular puncture. In the recipients, we detected GFP^+ cells preferentially located adjacent to the injured cites. GFP^+ cells in recipient cardiac tissues included $CD45^+$ or $CD11b^+$ hematopoietic cells (Figure 1A), $vimentin^+$ fibroblasts (Figure 1B), cardiac troponin I $(TnI)^+$ and/or Connexin 43 $(Cx43)^+$ cardiomyocytes (Figure 1C and 1D) indicating that the system could be used for analyzing differentiative and regenerative properties of donor stem/progenitor cells. Cardiomyocytes were counted by their specific intracellular striated structure and longer diameter compared with hematopoietic cells. Immunofluorescence studies confirmed that the counted cells were cardiomyocytes as evidenced by the expression of TnI. Since the frequencies of GFP^+ cardiomyocytes were similar in recipients transplanted with total BM cells or in those transplanted with $Lin^{-/low}$ MNCs, we postulated that the cardiomyogenic cells in BM are enriched in immature $Lin^{-/low}$MNCs.

BM-derived Cardiomyocytes Originate from the Hematopoietic Lineage

We next determined the contribution of HSCs and MSCs, two already-defined stem cells in BM, to the generation of GFP^+ cardiomyocytes. Multi-lineage differentiation capacities of HSCs included in the $CD45^+$ fraction and MSCs included in the $CD45^-$ fraction were confirmed by the development of lymphoid and myeloid cells *in vivo* and the induction of osteoblasts and adipocytes *in vivo* and *in vitro*, respectively (see Figure S1). To compare the cardiomyogenic abilities, 1.8×10^6–4.4×10^7 $Lin^{-/low}CD45^+$ cells and 3.6×10^5–2.5×10^6 $Lin^{-/low}CD45^-$ cells from GFP mice were transplanted into syngeneic recipients. At 4–6 weeks after transplantation, GFP^+ cardiomyocytes were detected only in recipients transplanted with $Lin^{-/low}CD45^+$ cells ($n=6$). By contrast, GFP^+ cardiomyocytes were not detected in recipients transplanted with $Lin^{-/low}CD45^-$ cells ($n=4$; $P=0.0095$ $Lin^{-/low}CD45^+$ versus $Lin^{-/low}CD45^-$; Table 1) nor in the recipient transplanted with purified $GFP^+Lin^-CD45^-$ cells. These findings suggest that donor-derived cardiomyocytes following BM transplantation originate from the hematopoietic lineage at least in this transplantation setting.

Transplantation of Purified BM HSC Fraction Resulted in the Efficient Production of Donor-derived Cardiomyocytes

Next, we aimed to assess the cardiomyogenic ability of purified hematopoietic stem/progenitor population. We transplanted limiting numbers of $GFP^+Lin^{-/low}Sca1^+$ cells including HSCs and hematopoietic progenitors, purified $GFP^+Lin^-Sca\text{-}1^+c\text{-}Kit^+$ cells (LSKs; Figure 2A) including HSCs and multipotent progenitors, and purified $GFP^+CD34^-Lin^-Sca\text{-}1^+c\text{-}Kit^+$ cells ($CD34^-$LSKs; Figure 2A) which contain HSCs that have long-term self-renewing potential. In all recipients transplanted with above three types of cells, GFP^+ cells of myeloid lineage, B cell lineage, and T cell lineage were present in peripheral blood (PB) and BM (see Figure S2). The numbers of GFP^+ cardiomyocytes significantly correlated with the injected cell dose in each group of the recipients transplanted with 10^3–10^6 $Lin^{-/low}Sca\text{-}1^+$ cells from GFP mice, 10^3–1.8×10^5 GFP^+LSKs, and 1–10^3 GFP^+CD34^-LSKs ($P<0.05$ in all groups; Figure 2C–E, Table 1). Furthermore, the incidence of GFP^+ cardiomyocytes per injected cell dose was greatest in GFP^+CD34^-LSKs recipients followed by that in GFP^+LSKs recipients, and the incidence in $GFP^+Lin^{-/low}Sca\text{-}1^+$ recipients was the lowest (Figure 2F, Table 1). GFP^+ cardiomyocytes were detected following transplantation of as few as 10 GFP^+CD34^-LSKs. We further confirmed contribution of self-renewing HSCs to the generation of cardiomyocytes by secondary and tertiary BM transplantation from GFP^+LSK recipients (see Table S1). These findings indicate that BM cells with cardiomyogenic capacity are highly enriched within the $CD34^-$LSK HSC population.

Myeloid Lineage Cells are the Primary Intermediates for Generating Cardiomyocytes

Since the capacity of HSCs to convert directly into cardiomyocytes has yet to be determined [18–21], we examined the capacity of hematopoietic progenitors to act as relevant intermediates for cardiomyogenesis. At 4 weeks after transplantation of 1.2×10^4–1.4×10^6 fluorescence-activated cell sorting (FACS)-purified $GFP^+Lin^-Thy1.2^-Sca\text{-}1^{-/low}c\text{-}Kit^{+/low}$ cells which mainly contain mixed myeloid and lymphoid progenitor population, GFP^+ cardiomyocytes were identified in all recipients ($n=10$; Table 1). This result indicates that transplanted HSCs give rise to cardiomyocytes via hematopoietic intermediates, at least partly.

To discriminate the hematopoietic lineage required in cardiomyogenesis, we then transplanted 0.4–2.8×10^5 FACS-purified $GFP^+Lin^-Thy1.2^-$interleukin-7 receptor α-chain $(IL\text{-}7R\alpha)^-Sca\text{-}1^-c\text{-}Kit^+$ total myeloid progenitors ($n=7$) and 0.2–3.3×10^5 $GFP^+Lin^-Thy1.2^-IL\text{-}7R\alpha^+Sca\text{-}1^{low}c\text{-}Kit^{low}$ common lymphoid progenitors (CLPs; $n=9$) sorted simultaneously from the same GFP^+ BM cells (Figure 2B). At 3–6 weeks after transplantation, recipients of myeloid progenitors showed predominant GFP^+

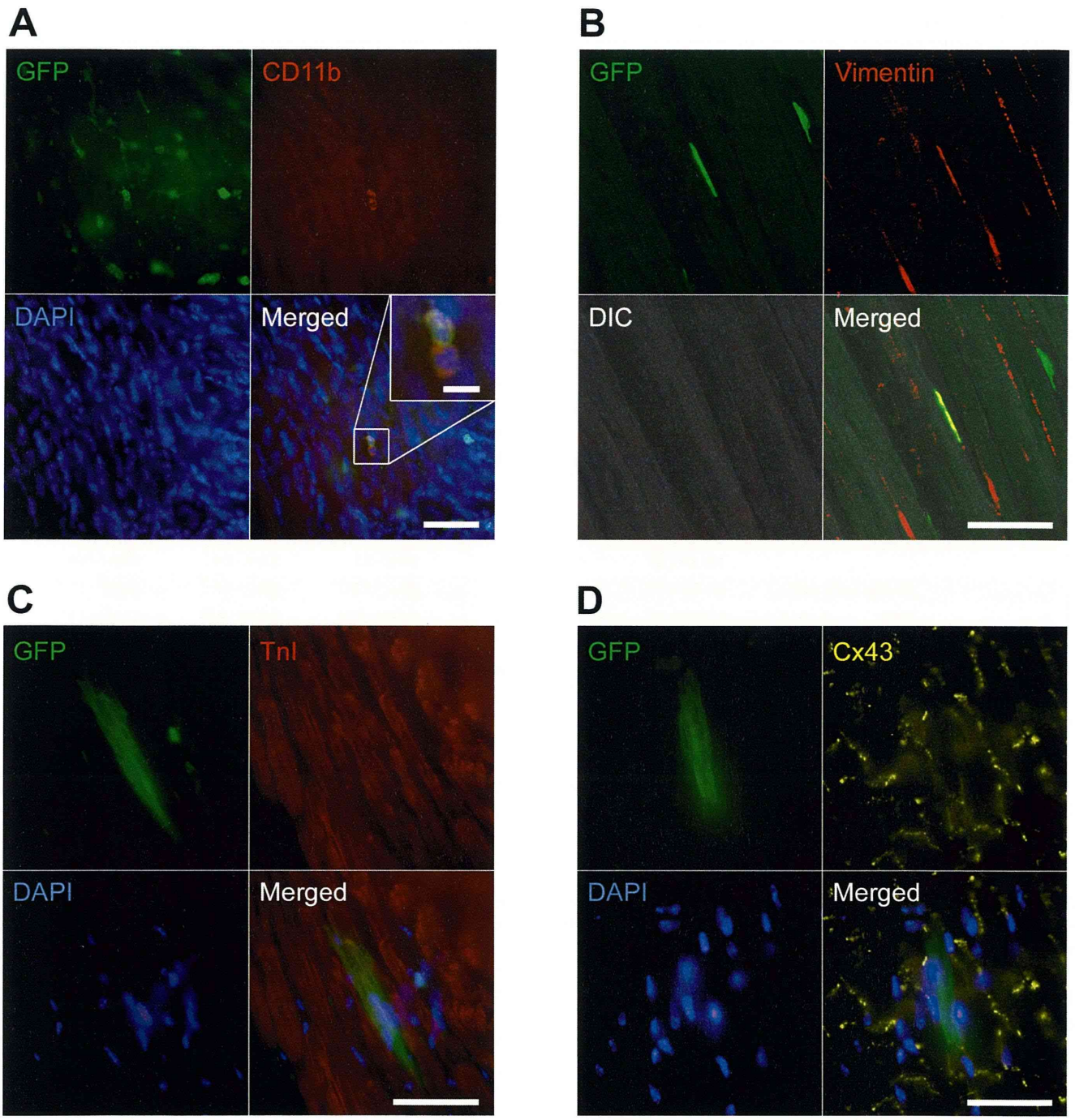

Figure 1. Characterization of donor BM-derived GFP$^+$ cells in injured heart. (A) Representative image of CD11b-expressing GFP$^+$ myeloid cells. GFP$^+$ hematopoietic cells in recipient cardiac tissue appeared in small and round shape. Cardiac section was stained with anti-CD11b (red, Cy3) and DAPI (blue). Inset: high magnification of GFP$^+$CD11b$^+$ cells. (B) Representative image of a vimentin-expressing GFP$^+$ fibroblast. Cardiac section was stained with anti-vimentin (red, Cy3). The fibroblast was present adjacent to striated cardiomyocytes in differential interference contrast (DIC) image. (C and D) Representative images of a TnI- (C) or Cx43- (D) expressing GFP$^+$ striated cardiomyocyte. Cardiac sections were stained with anti-TnI (C; red, Cy3), anti-Cx43 (D; yellow, Cy5), and DAPI (blue). Cardiac sections are from recipients transplanted with unfractionated BM cells. All merged images were obtained from the same confocal plane. Scale bars = 50 μm, (A)-inset 10 μm.
doi:10.1371/journal.pone.0062506.g001

myeloid engraftment while recipients of CLPs showed predominant GFP$^+$ lymphoid engraftment in PB (see Figure S2). Although recipients of myeloid progenitors and CLPs showed similar PB GFP$^+$ engraftment (Table 1), significantly greater number of GFP$^+$ cardiomyocytes were identified in recipients transplanted with myeloid progenitors than in those transplanted with CLPs ($P = 0.0021$; Table 1). We further confirmed the contribution of myeloid cells to the generation of cardiomyocytes by transplantation of GFP$^+$Lin$^-$IL-7Rα$^-$Sca-1$^-$c-Kit$^+$ Fcγ receptor-II/III (FcγR)^{low}CD34$^+$ common myeloid progenitor (CMPs; 0.3–1.0×10^5, $n = 6$; Table 1) and GFP$^+$Lin$^-$IL-7Rα$^-$Sca-1$^-$c-Kit$^+$FcγR^{high}CD34$^+$ granulocyte/monocyte progenitors (GMPs;

Table 1. The number of donor-derived cardiomyocytes after transplantation of purified BM cells.

Donor cell type		Cell dose	n	Days after injection	BM %GFP$^+$	PB %GFP$^+$	GFP$^+$ cardiomyocytes*
Hematopoietic cell	Lin$^{-/low}$CD45$^+$	0.2–4.4×10^7	6	25–46	86.7+/−13.9	90.6+/−5.6	37.0+/−23.9[a]
Mesenchymal cell	Lin$^{-/low}$CD45$^-$	0.4–2.5×10^6	4	25–39	0.35+/−0.39	0.03+/−0.05	0.00+/−0.00[a]
HSC	Lin$^{-/low}$Sca-1$^+$	10^6	5	29–34	83.2+/−6.6	96.4+/−2.9	33.9+/−16.0
		10^5	5	29–39	54.8+/−17.8	75.5+/−17.0	21.8+/−10.7
		10^4	5	28–39	3.0+/−1.6	6.0+/−7.6	4.2+/−3.4
		10^3	5	28–39	0.59+/−0.40	1.6+/−2.5	1.2+/−1.1
	LSK	1.0–1.8×10^5	6	27–44	76.6+/−17.7	89.1+/−17.0	33.6+/−43.1
		1.0–4.0×10^4	8	31–52	36.2+/−25.1	45.0+/−32.8	9.3+/−10.3
		1.0–2.0×10^3	6	31–52	25.5+/−23.3	38.2+/−27.6	2.4+/−2.0
	CD34$^-$LSK	10^3	2	28–50	66.8+/−27.3	67.3+/−23.6	12.5+/−5.0
		10^2	3	31–57	6.7+/−10.9	15.5+/−14.9	3.4+/−2.5
		10	7	213–354	0.19+/−0.13	0.05+/−0.05	0.14+/−0.38
		1	34	116–378	0.12+/−0.21	0.06+/−0.09	0.00+/−0.00
Hematopoietic progenitor	Lin$^-$Thy1.2$^-$Sca-1$^{-/low}$c-kit$^{+/low}$	1.2–1.4×10^6	3	29–31	62.9+/−18.7	82.3+/−4.4	16.9+/−8.2
		1.2–4.7×10^5	3	27–29	37.9+/−21.3	51.8+/−27.5	14.4+/−7.4
		1.2–3.0×10^4	4	21–29	4.6+/−5.3	3.8+/−2.4	10.8+/−4.4
	Myeloid progenitor	0.4–2.8×10^5	7	24–39	4.2+/−5.2	3.6+/−4.1 [d]	12.8+/−10.7[b]
	CMP	0.3–1.0×10^5	6	31–42	0.87+/−0.70	0.52+/−0.59	17.2+/−7.3 [c]
	GMP	0.9–1.3×10^5	4	24–42	1.5+/−2.4	11.0+/−22.0	6.6+/−5.9
	CLP	0.2–3.3×10^5	9	24–39	4.0+/−4.7	8.7+/−6.8[d]	0.67+/−1.00[b,c]

[a]P = 0.0095 by Mann-Whitney U test, Lin$^{-/low}$CD45$^+$ versus Lin$^{-/low}$CD45$^-$.
[b]P = 0.0021 by Mann-Whitney U test, Myeloid progenitor versus CLP.
[c]P = 0.0004 by Mann-Whitney U test, CMP versus CLP.
[d]P = 0.1142 by Mann-Whitney U test, Myeloid progenitor versus CLP.
*GFP$^+$ cardiomyocytes were counted in 40 contiguous sections from apex of the heart per a mouse. Detailed information of histological analysis is described in Materials and Methods, Materials and Methods S1.
Abbreviations. BM: bone marrow, PB: peripheral blood, HSC: hematopoietic stem cell, LSK: Lin$^-$Sca-1$^+$c-Kit$^+$, CMP: common myeloid progenitor, GMP: granulocyte/monocyte progenitor, CLP: common lymphoid progenitor.
doi:10.1371/journal.pone.0062506.t001

0.9–1.3×10^5, n = 4; Table 1). These findings suggest that myeloid derivatives are responsible for providing cardiomyocytes in recipients.

Cell Fusion is the Major Mechanism Underlying the Generation of BM-derived Cardiomyocytes

To explore the mechanism of BM-derived cardiomyocyte generation, BM cells of GFP mice were transplanted into cyan fluorescence protein (CFP)-transgenic newborn mice. At 4–22 weeks after transplantation of unfractionated BM cells, LSK, Lin$^-$Thy1.2$^-$Sca-1$^{-/low}$c-Kit$^{+/low}$, Lin$^{-/low}$Sca-1$^+$, and Lin$^{-/low}$-Sca-1$^-$ cells from GFP mouse BM, 1–166 GFP$^+$ cardiomyocytes per a mouse were detected in CFP recipients (n = 11). The incidence of GFP$^+$ cardiomyocytes in CFP recipients was comparable to that in C57BL/6 recipients, suggesting that the cardiomyogenic event is not influenced by employing CFP-transgenic mice as recipients. The emitted fluorescence from recipient cardiac sections stained with cardiac TnI-cyanin-3 (Cy3), Cx43-cyanin-5 (Cy5), and 4′,6-diaimidino-2-phenylindole (DAPI) was detected at 10–11 nm interval from 417 nm to 749 nm wavelength using a laser-scanning confocal microscope (Figure 3A). The presence of cyan fluorescence in multiple points of each GFP$^+$TnI$^+$Cx43$^+$ cardiomyocyte was examined by using linear unmixing analysis (see Materials and Methods S1). Irrespective of the donor cell type, all 21 GFP$^+$ cardiomyocytes detected in the cardiac tissues of 8 recipients coexpressed CFP (Figure 3B and 3C, see Table S2), suggesting that BM-derived cardiomyocytes are generated through cell fusion between BM-derived cells and recipient-derived cardiomyocytes.

Analysis of Cardiomyocyte-specific Genes in Mice Transplanted with Human Cord Blood HSCs

Finally, we aimed to clarify whether donor hematopoietic cells can change their cell fate through cell fusion with host cardiomyocytes. To this end, we set up xenogeneic transplantation by injecting human cord blood-derived CD34$^+$CD38$^-$ HSCs into immune-compromised mice (NOD/SCID/IL2rγ^{null} mice [23], NOD.Rag1^{null}IL2rγ^{null} mice [24], and C57BL/6.Rag2^{null}IL2rγ^{null}NOD-Sirpa mice [25]). We extracted ribonucleic acid (RNA) from recipient cardiac tissues and performed quantitative real-time polymerase chain reaction (qRT-PCR) to detect human-specific cardiac transcription factors (Gata-4 [GATA4], Tbx 5 [TBX5], Nkx 2.5 [NKX2–5], and Mesp 1 [MESP1]) [26] and cardiomyocyte structural genes (α-myosin heavy chain 6 [MYH6] and cardiac troponin C [TNNC1], connexin 43 [GJA1], and ryanodine receptor 2 [RYR2]). Of cardiac transcription factors, Gata-4, Tbx 5, and Mesp 1 were not expressed in any of the examined 14 recipients. Although Nkx 2.5 was expressed in 2 of

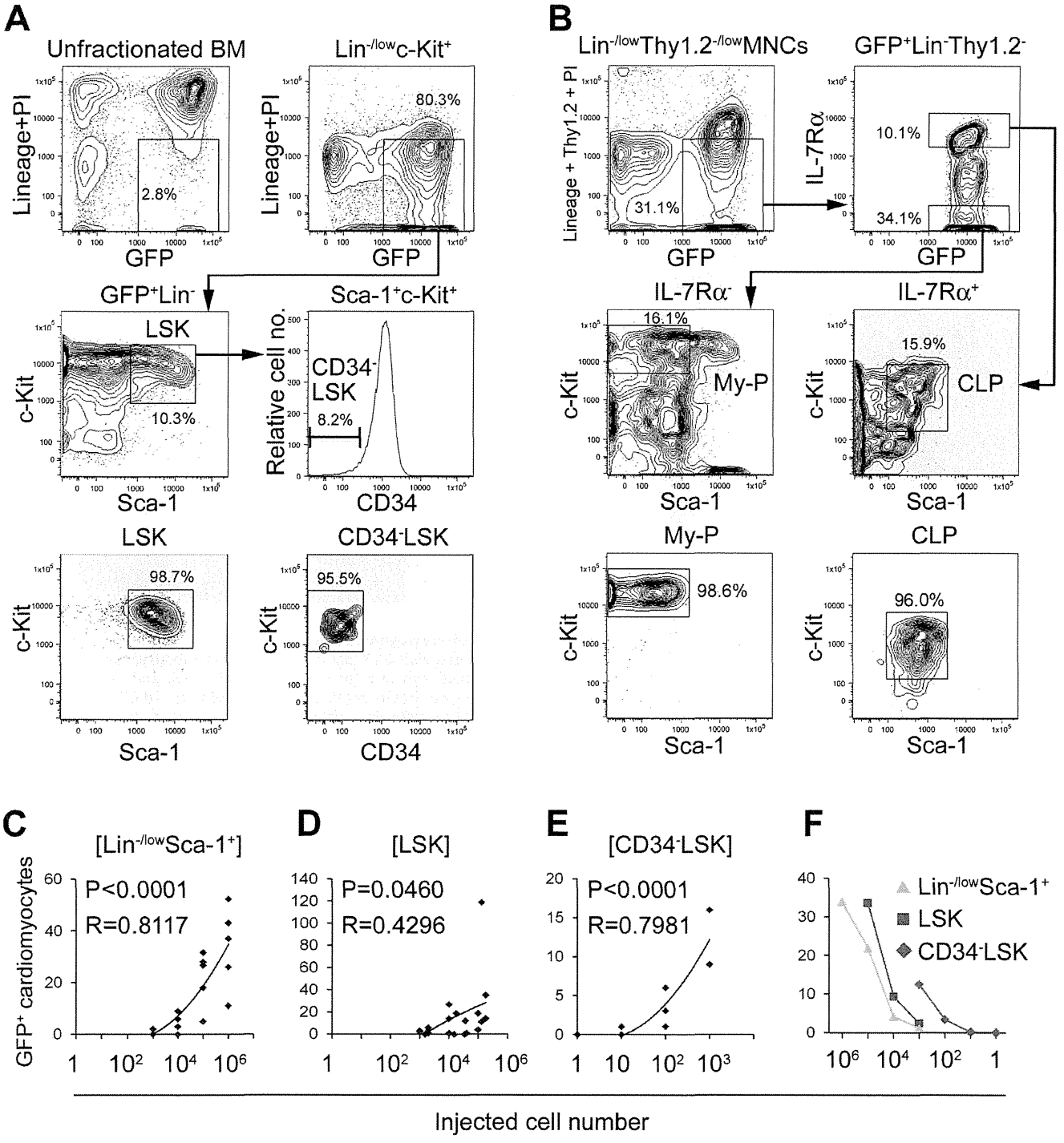

Figure 2. Transplantation of HSCs and hematopoietic progenitors. (A) LSKs or $CD34^-$LSKs were purified by FACS from $Lin^{-/low}$c-Kit^+ BM fraction of GFP mice. GFP and Lineage+propidium iodide (PI) expression of unfractionated BM cells is shown as a control. (B) Total myeloid progenitors (My-P) and CLPs were purified by FACS from $Lin^{-/low}Thy1.2^{-/low}$MNCs of GFP mice. (C-E) Correlational analyses between injected cell numbers and the numbers of GFP^+ cardiomyocytes per a recipient mouse in recipients transplanted with $Lin^{-/low}Sca\text{-}1^+$ cells (C), LSKs (D), and $CD34^-$LSKs (E). (F) Comparison of the number of GFP^+ cardiomyocytes at the same injected cell dose in $Lin^{-/low}Sca\text{-}1^+$ cells, LSKs, and $CD34^-$LSKs recipients. The means of the number of GFP^+ cardiomyocytes in recipients transplanted with each injected cell number are plotted. In the transplantation of LSKs, injected cell number of $1\text{–}1.8\times10^5$ cells is plotted at 10^5, that of $1\text{–}4\times10^4$ cells is plotted at 10^4, and that of $1\text{–}2\times10^3$ cells is plotted at 10^3. The greater cardiomyogenic ability existed in $CD34^-$LSKs than LSKs, and in LSKs than $Lin^{-/low}Sca\text{-}1^+$ cells.
doi:10.1371/journal.pone.0062506.g002

14 recipients, the expression of Nkx 2.5 was not specific to human cardiomyocytes since it was expressed in human cord blood [27] (see Table S3). Of cardiomyocyte structural genes, human myosin heavy chain 6 and troponin C were expressed in 1 of 14 and 9 of 14 recipients, respectively. Specificity of these probes to human cardiomyocytes was confirmed by the positive reaction to human

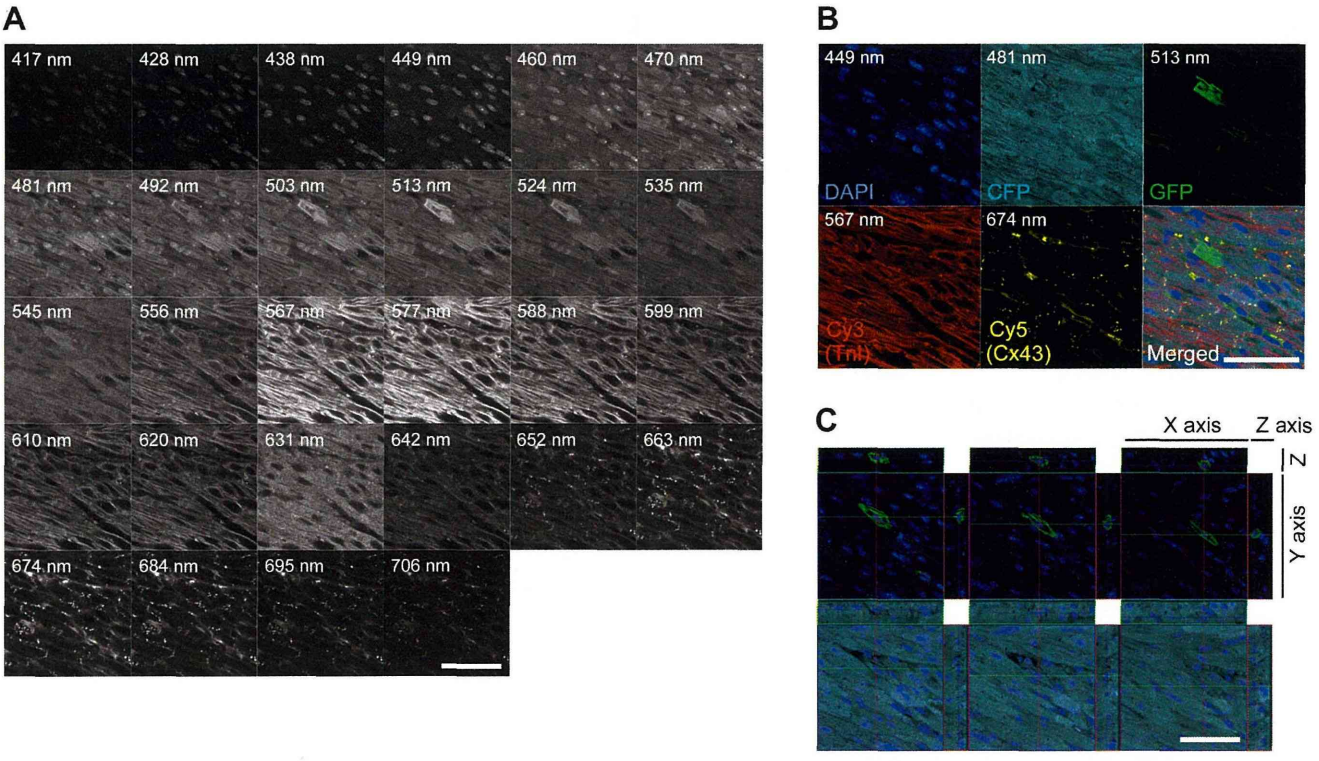

Figure 3. CFP expression in the GFP$^+$ BM-derived cardiomyocyte of a CFP-transgenic recipient mouse. (A) Representative image of fluorescence detection from cardiac tissue of the CFP-transgenic recipient transplanted with GFP$^+$ BM cells. Detected fluorescence images between 417 and 706 nm wavelength at 10–11 nm interval from a cardiac section stained with anti-TnI (Cy3), anti-Cx43 (Cy5), and DAPI are shown sequentially. (B) The expressions of DAPI, CFP, GFP, Cy3, and Cy5 in the cardiomyocyte shown in (A). Composition of GFP and CFP was examined simultaneously from each detected image between 449 and 663 nm wavelength (linear unmixing analysis). Detection wavebands used to visualize each fluorescence are described in each fluorescence image. The cardiomyocyte shown in (A) expressed donor-derived GFP, recipient-derived CFP, cardiac TnI, and Cx43. (C) Three dimensional analysis of the cardiomyocyte shown in (A) and (B) at the position of each nucleus. In every cross-section of three planes including nuclei, this cardiomyocyte expressed both GFP and CFP. Merged images (B and C) were obtained from the same confocal plane. Scale bars = 20 μm.
doi:10.1371/journal.pone.0062506.g003

heart and the negative reaction to mouse heart and human cord blood. By contrast, ryanodine receptor 2 was not detected in any cardiac specimens derived from human HSC-engrafted recipients. Although connexin 43 was expressed in all of the recipients, the expression of connexin 43 was not specific to human cardiomyocytes since it was expressed in human cord blood consistent with previous reports showing connexin expression on several hematopoietic cells [28] (see Table S3). Although the frequency of cell fusion between donor hematopoietic cells and host cardiomyocytes is extremely low, we detected the cardiomyocyte-specific expression of the human cardiomyocyte structural gene, cardiac troponin C, but not that of other human cardiomyocyte structural genes such as ryanodine receptor 2 or human cardiac transcription factors in the cardiac tissue of recipient mice.

Discussion

We have obtained three findings by tracing the fate of genetically marked BM cells *in vivo*. First, HSCs generate cardiomyocytes along with hematopoietic reconstitution. Second, myeloid lineage cells are primary intermediates for cardiomyocyte generation. Third, cell fusion with recipient-derived cardiomyocytes is required for the generation of BM-derived cardiomyocytes. In this study, transplantation of cells derived from GFP-transgenic mouse into CFP-transgenic recipients enabled us to determine the mechanism for the generation of donor marker-positive cardiomyocytes. Moreover, confocal imaging and analyses for the separation of these two fluorescences led us to address the long-term question as to the issue of cell fusion or transdifferentiation.

Transplantation of purified HSCs to newborn syngeneic mice with cardiac injury resulted in the most frequent appearance of donor-marker$^+$ cardiomyocytes in cardiac tissues. The results suggest the two possibilities, direct contribution of HSCs to cell fusion with cardiomyocytes and cell fusion between myeloid progeny and cardiomyocytes. Previous reports suggest that purified HSCs do not generate cardiomyocytes when directly transplanted into myocardium [10,20,21], but can generate cardiomyocytes following BM transplantation at a low frequency [4,10,12]. We have shown that cell fusion between BM-derived myeloid cells and host-derived cardiomyocytes results in the generation of donor-marker$^+$ cardiomyocytes. The frequency of BM-derived cardiomyocytes in our study (~0.04%, see Materials and Methods S1) and other rodent studies (0.001–0.02%) [4,10,20] are similar to those of host marker-expressing cardiomyocytes in human cardiac transplantation (0.04–0.16%) [29,30], which may be the frequency of fusion between circulating myeloid cells from BM and cardiomyocytes in mammals in general.

Cells of myeloid lineage have been shown to contribute to skeletal myocytes [31,32], hepatocytes [33,34], or vascular endothelium [35] *in vivo*. We report here contribution of BM-derived myeloid progenitors to the generation of cardiomyocytes. Actually, several plasma membrane molecules related with cell

fusion were up-regulated in myeloid lineage cells than lymphoid lineage cells confirmed by qRT-PCR (see Figure S3). Expression levels of integrin beta 1 [Itgb1] or signal-regulatory protein alpha [Sirpa] in CMP were 1.73 or 1.82 fold higher than those in CLP, respectively (n = 3). Of the cells derived from GMPs, monocytic cells are likely candidates as fusion partners since they have a physiological capacity for cell fusion [36]. Based on the finding that $CD11b^{low}$ cells, rather than $CD11b^{high}$ cells, within $Gr\text{-}1^{-/low}c\text{-}Kit^{-}$ BM fraction generated cardiomyocytes (unpublished observations), $CD11b^{low}$ immature monocytes may be the population contributing to the appearance of donor-$marker^{+}$ cardiomyocytes similar to the previous report describing the regeneration of skeletal muscle [32].

The number of donor-derived cells in recipient BM was very low following the transplantation of $Lin^{-/low}CD45^{-}$ cells in our study (Table 1), consistent with previous studies [37,38]. Mesenchymal stem cells in the BM are considered to be relatively resistant to irradiation compared with HSCs [37,38]. Therefore, the lack of donor-derived cardiomyocytes following systemic infusion of $Lin^{-/low}CD45^{-}$ cells into sublethally irradiated mice may be due to inefficient engraftment of injected MSCs in the recipient BM. Intra-BM injection of 10^5 GFP-labeled clonally purified MSCs (CMG cells) resulted in the generation of donor-$marker^{+}$ cardiomyocytes [11]. Our results, together with the report showing little ability of MSCs to give rise to cardiomyocytes following intravenous or intramyocardial transplantation [8], imply that administration route and cell preparation need to be extensively assessed for cell therapy using MSCs. We examined whether BM-derived mesenchymal cells gain a cardiomyocyte phenotype through differentiation or cell fusion with a coculture experiment using GFP-expressing BM mesenchymal cells and adult cardiomyocytes. In the experiment, one GFP^{+} cell expressing cardiomyocyte-specific antigens was detected (unpublished observations). However, the function of the cardiac-maker positive cell as a cardiomyocyte is unknown. A previous study demonstrated that mesenchymal stromal cell-derived cells acquiring cardiomyocyte phenotypic characteristics do not exhibit sufficient electrical property [39]. Additionally, improvement of cardiac function via mesenchymal stem/stromal cell transplantation is thought to be mediated by paracrine mechanism in addition to the direct contribution of cardiac marker-positive mesenchymal stem/stromal cells in themselves as contractile cardiomyocytes [40,41]. Recent report suggests that mesenchymal stromal cells recruit monocytes/macrophages secreting IL-10 or TGF-β [41]. Macrophages contributing to anti-inflammatory status could be one of the determinants for tissue regeneration in a mouse model for myocardial infarction [41]. Therefore, whether HSCs and MSCs act synergistically to regenerate cardiac tissue or to inhibit apoptosis in damaged cardiac tissue should be evaluated by using a large animal model in the future.

To establish regenerative medicine for heart failure patients, long-term improvement in cardiac function is important. Self-renewing cardiac-resident stem/progenitor cells [42,43] could maintain a pool for cardiomyocyte turnover [44,45]. BM could be one of the reservoirs that can give rise to cardiac-resident stem cells [46] and cells of multiple lineages [47]. Indeed, cardiomyocyte renewal in adult mammals is demonstrated under the physiological condition [48] or after injury [1]. Therefore, it should be demonstrated in the future to what degree BM-derived stem/progenitor cells and cardiac stem/progenitor cells contribute to turnover and regeneration of cardiomyocytes in the physiological or pathological conditions and whether BM-derived stem/progenitor cells can generate cardiac stem/progenitor cells.

Finally, we have demonstrated the contribution of myeloid lineage cells to cardiomyocytes through cell fusion. Recent reports suggest that stem cell fusion with the cardiomyocyte could add contractile function to the injured heart [49], and BM cell transplantation can restore impaired cardiac function [7]. Identification of the specific cell type and factors involved in cell fusion may lead to the enhancement of therapeutic effects of ongoing clinical cell therapy. In our qPCR analysis, two out of 6 donor cardiomyocyte-specific genes were detected in recipient cardiac tissues. Considering the low frequency of cell fusion, future *in vitro* and *in vivo* experiments might be required to determine as to how far reprogramming process occurs following cell fusion. Altogether, our findings suggest that myeloid progenitors may potentially serve as a readily available source of effecter cells for targeted cellular therapy of cardiac disorders through cell fusion.

Materials and Methods

Mice

C57BL/6 mice transgenically expressing enhanced GFP driven by the cytomegalovirus (CMV) enhancer/chicken β-actin promoter were kindly provided by Dr. M. Okabe (Osaka University). C57BL/6 mice transgenically expressing enhanced CFP driven by the CMV enhancer/chicken β-actin promoter, NOD/SCID/$IL2r\gamma^{null}$ mice, and NOD.$Rag1^{null}IL2r\gamma^{null}$ mice were obtained from the Jackson Laboratory (Bar Harbor, ME). C57BL/6.$Rag2^{null}IL2r\gamma^{null}$NOD-Sirpa mice were generated in our laboratory. All mice were bred and maintained under defined flora. Experiments were performed according to the guidelines approved by the Institutional Animal Committee of Kyushu University (Approval ID: 18–68). PB sampling from recipient mice was performed under deep inhalation anesthesia. BM and heart were dissected out from donor/recipient mice sacrificed by cervical dislocation under deep inhalation anesthesia.

Purification of Donor Cells

BM cells were harvested from GFP-transgenic mice at 8–12 weeks of age by flushing femurs and tibiae. MNCs were isolated by gradient centrifugation. Rat anti-mouse lineage antigen (BD Pharmingen, Caltag) and sheep anti-rat IgG antibody-conjugated immunomagnetic beads (Dynal) were used to deplete mature hematopoietic cells from MNCs. For separation of $Lin^{-/low}CD45^{+}$ cells and $Lin^{-/low}CD45^{-}$ cells and enrichment of $Lin^{-/low}Sca\text{-}1^{+}$ cells or $Lin^{-/low}c\text{-}Kit^{+}$ cells by magnetic cell sorting, immunomagnetic microbeads (Miltenyi Biotec) were used. For purification of each BM stem/progenitor fraction by FACS, enriched BM cells were labeled by fluorescence-conjugated antibodies (see Materials and Methods S1). Umbilical cord blood cells were collected during normal full-term delivers after obtained written informed consent (provided by Kyushu Block Red Cross Blood Center, Japan Red Cross Society). Experiments using cord blood were performed according to the guidelines approved by the Institutional Committee of Kyushu University (Approval ID: 17–114). MNCs were separated by Ficoll-Hypaque density-gradient centrifugation. Lineage-depleted cord blood cells were obtained magnetically (Miltenyi Biotec). Sorting of $CD34^{+}CD38^{-}$ subfractions was accomplished by staining lineage-depleted cord blood cells with fluorescein isothiocyanate (FITC)-conjugated anti-CD34, and phycoerythrin (PE)-conjugated anti-CD38 (BD Biosciences). Cell sorting was performed on a FACSAria (BD).

Transplantation

Unfractionated or purified BM cells from GFP mice were injected intravenously into C57BL/6 mice or CFP-transgenic mice

within 48 hours of birth after 560 cGy irradiation. Left ventricular wall injury was induced by puncturing newborn recipient heart with a 29 G needle following transplantation of donor BM cells. Five to ten thousand $Lin^-CD34^+CD38^-$ cells from human cord blood were transplanted into immune-compromised mice after irradiation.

Flow Cytometric Analysis of Recipient PB and BM

PB was collected from retro-orbital plexus of recipients, and BM cells were harvested from femurs and tibiae. The percentage of GFP^+ cells in PB and BM of recipients was examined by flow cytometric analysis using FACSCalibur (BD). PB and BM of recipients were labeled with each biotin-conjugated anti-mouse lineage antigen (CD3e, CD11b, B220, Gr-1, and TER-119) antibody, subsequently labeled with Cy3-conjugated streptavidin (Jackson ImmunoResearch) to recognize myeloid cells (CD11b, Gr-1), T lymphocytes (CD3e), and B lymphocytes (B220) by flow cytometric analysis. FACS lysing solution (BD) was used to lyse red blood cells following antibody labeling.

Histological Analysis

Recipient hearts were removed and perfused with PBS to eliminate blood cells immediately after they were sacrificed by cervical dislocation. For immunofluorescence staining, recipient hearts were sectioned into 100-μm slices from apex to base with a vibratome (DTK-1000, D.S.K.) following fixation in 4% paraformaldehyde and dehydration in 70% ethanol. Vibratome-sectioned cardiac slices were stained with primary antibodies to CD45 (DakoCytomation), CD11b (BD Pharmingen), vimentin (Sigma), cardiac troponin I (TnI; Santa Cruz Biotechnology), and connexin43 (Cx43; Chemicon). Secondary antibodies conjugated with Cy3 or Cy5 (Jackson ImmunoResearch) were used to visualize primary antibodies. Forty contiguous cardiac sections per a recipient mouse were carefully examined for the presence of GFP^+ cardiomyocytes by laser-scanning confocal microscopy (LSM-GB200, Olympus). In the transplantation of GFP^+ BM cells into CFP-transgenic mice, linear unmixing analysis was employed to distinguish GFP^+ donor-derived cells, GFP^+CFP^+ fused cells, and CFP^+ recipient-derived cells as described previously [12] (LSM510 META, Carl Zeiss, see Materials and Methods S1).

Quantitative Real-time Polymerase Chain Reaction

Total RNA was extracted from recipient heart, non-recipient mouse heart, human cord blood, and 10^4 cells each of sorted mouse hematopoietic cells. Reverse transcription was performed using SuperScript II or SuperScript III (Invitrogen) according to the manufacturer's instructions. For human-specific cardiac transcription factors and cardiomyocyte structural genes, qRT-PCR was performed on the synthesized complementary deoxyribonucleic acid (cDNA) with Platinum Quantitative PCR SuperMix (Invitrogen) on LightCycler 480 (Roche) to determine cycle thresholds (C_T) of amplification. Human heart QUICK-Clone cDNA (Clontech) was used as a positive control. Human glyceraldehyde-3-phosphate dehydrogenase (GAPDH) was used as the internal control. For mouse adhesion molecules, qRT-PCR was performed on Applied Biosystems 7500 real-time PCR system with TaqMan(R) primer-probe sets provided from Applied Biosystems. 18 s rRNA was used as the internal control. Sequences of dual-labeled fluorogenic probes and gene-specific primers (Sigma-Aldrich), and product ID of TaqMan(R) Gene Expression Assay (Applied Biosystems) are listed on Table S4. For initial normalization to the housekeeping gene, the difference in C_T value (ΔC_T = [C_T gene of interest] − [C_T human GAPDH or 18 s rRNA]) was determined on each sample. Relative expression levels of each mRNA were calculated as the ratio to levels of human heart or mouse CLP cDNA using the comparative C_T ($2^{-\Delta\Delta C_t}$) method [50].

Statistical Analysis

Results are presented as mean +/− standard deviation (S.D.). Probability values were calculated by using the Mann-Whitney U test (non-parametric independent two-group comparison) or the Pearson's correlation coefficient test. A probability value of less than 0.05 was considered to be statistically significant.

Supporting Information

Figure S1 Differentiation capacities of $Lin^{-/low}CD45^-$ cells. (A) CD45 expression of $Lin^{-/low}$MNCs, separated $Lin^{-/low}CD45^+$ cells, and separated $Lin^{-/low}CD45^-$ cells. (B) Bright-field and fluorescence image of $GFP^+Lin^{-/low}CD45^-$ cells following culture. Polygonal or spindle-shaped adherent GFP^+ cells were recognized as mesenchymal cells. (C) *In vitro* differentiation of $Lin^{-/low}CD45^-$ cells into osteoblasts (left) or adipocytes (right) by induction using differentiation media for each. Differentiation into osteoblasts or adipocytes was confirmed by alkaline phosphatase staining (left; red) or Oil red O staining (right; lipid vacuoles are stained in red), respectively. (D) Bone section of recipients transplanted with $GFP^+Lin^{-/low}CD45^-$ cells stained with anti-GFP (red, Cy3), anti-CD45 (yellow, Cy5), and DAPI (blue). Bright-field image is shown at leftmost. GFP^+CD45^- cells were present within bone cortex (white arrows). These results suggest that separated $Lin^{-/low}CD45^-$ cells contain MSCs that can differentiate into multiple mesenchymal lineages. Merged images were obtained from the same confocal plane. Scale bars = 20 μm.
(TIF)

Figure S2 Flow cytometric analysis of recipient hematopoietic tissues. Representative image of flow cytometric analysis of recipient PB and BM transplanted with FACS-purified LSKs, and recipient PB transplanted with total myeloid progenitors (My-P) or CLPs. In LSK recipients, donor-derived GFP^+ myeloid cell lineage ($Gr\text{-}1^+$ or $CD11b^+$), B cell lineage ($B220^+$), and T cell lineage ($CD3e^+$) were confirmed. Donor-derived myeloid cell lineage ($Gr\text{-}1^+$ or $CD11b^+$) was predominantly present in recipients transplanted with total myeloid progenitors, and donor-derived B/T cell lineage ($B220^+$ or $CD3e^+$) was predominantly present in recipients transplanted with CLPs.
(TIF)

Figure S3 Relative cDNA expression of adhesion molecules in myeloid and lymphoid lineages. The averages of relative cDNA expressions from three qRT-PCR experiments are indicated by histogram with positive standard deviation. Expression levels of Itgb1 and Sirpa in CMP were higher than those in CLP. Expression levels of Itgb1, Sirpa, and Adam9 in myeloid derivatives (neutrophil, monocyte) were higher than those in lymphoid derivatives (T lymphocyte, B lymphocyte). In the four adhesion molecules examined (Itgb1, Sirpa, Adam9, and Adam12), Adam12 was not detected in any of the samples. Gene names corresponding to each gene symbol, probes and primers information are described in Table S4.
(TIF)

Table S1 The number of donor-derived cardiomyocytes after serial transplantation.
(XLS)

Table S2 CFP expression of donor-derived GFP^+ cardiomyocytes in CFP recipient mice.
(XLS)

Table S3 Relative cDNA expression to human heart.
(XLS)

Table S4 Probes and primers for quantitative real-time polymerase chain reaction (qRT-PCR).
(XLS)

Materials and Methods S1 Detailed information on purification of donor BM cells, cell culture and differentiation assay of $Lin^{-/low}CD45^-$ cells, and histological analysis.
(DOC)

References

1. Hsieh PC, Segers VF, Davis ME, MacGillivray C, Gannon J, et al. (2007) Evidence from a genetic fate-mapping study that stem cells refresh adult mammalian cardiomyocytes after injury. Nat Med 13: 970–974.
2. Dimmeler S, Zeiher AM, Schneider MD (2005) Unchain my heart: the scientific foundations of cardiac repair. J Clin Invest 115: 572–583.
3. Orlic D, Kajstura J, Chimenti S, Jakoniuk I, Anderson SM, et al. (2001) Bone marrow cells regenerate infarcted myocardium. Nature 410: 701–705.
4. Jackson KA, Majka SM, Wang H, Pocius J, Hartley CJ, et al. (2001) Regeneration of ischemic cardiac muscle and vascular endothelium by adult stem cells. J Clin Invest 107: 1395–1402.
5. Schächinger V, Erbs S, Elsässer A, Haberbosch W, Hambrecht R, et al. (2006) Intracoronary bone marrow-derived progenitor cells in acute myocardial infarction. N Engl J Med 355: 1210–1221.
6. Meyer GP, Wollert KC, Lotz J, Steffens J, Lippolt P, et al. (2006) Intracoronary bone marrow cell transfer after myocardial infarction: eighteen months' follow-up data from the randomized, controlled BOOST (BOne marrOw transfer to enhance ST-elevation infarct regeneration) trial. Circulation 113: 1287–1294.
7. Jeevanantham V, Butler M, Saad A, Abdel-Latif A, Zuba-Surma EK, et al. (2012) Adult bone marrow cell therapy improves survival and induces long-term improvement in cardiac parameters: a systematic review and meta-analysis. Circulation 126: 551–568.
8. Breitbach M, Bostani T, Roell W, Xia Y, Dewald O, et al. (2007) Potential risks of bone marrow cell transplantation into infarcted hearts. Blood 110: 1362–1369.
9. Koide Y, Morikawa S, Mabuchi Y, Muguruma Y, Hiratsu E, et al. (2007) Two distinct stem cell lineages in murine bone marrow. Stem Cells 25: 1213–1221.
10. Nygren JM, Jovinge S, Breitbach M, Säwén P, Röll W, et al. (2004) Bone marrow-derived hematopoietic cells generate cardiomyocytes at a low frequency through cell fusion, but not transdifferentiation. Nat Med 10: 494–501.
11. Kawada H, Fujita J, Kinjo K, Matsuzaki Y, Tsuma M, et al. (2004) Nonhematopoietic mesenchymal stem cells can be mobilized and differentiate into cardiomyocytes after myocardial infarction. Blood 104: 3581–3587.
12. Ishikawa F, Shimazu H, Shultz LD, Fukata M, Nakamura R, et al. (2006) Purified human hematopoietic stem cells contribute to the generation of cardiomyocytes through cell fusion. FASEB J 20: 950–952.
13. Toma C, Pittenger MF, Cahill KS, Byrne BJ, Kessler PD (2002) Human mesenchymal stem cells differentiate to a cardiomyocyte phenotype in the adult murine heart. Circulation 105: 93–98.
14. Terada N, Hamazaki T, Oka M, Hoki M, Mastalerz DM, et al. (2002) Bone marrow cells adopt the phenotype of other cells by spontaneous cell fusion. Nature 416: 542–545.
15. Alvarez-Dolado M, Pardal R, Garcia-Verdugo JM, Fike JR, Lee HO, et al. (2003) Fusion of bone-marrow-derived cells with Purkinje neurons, cardiomyocytes and hepatocytes. Nature 425: 968–973.
16. Weimann JM, Johansson CB, Trejo A, Blau HM (2003) Stable reprogrammed heterokaryons form spontaneously in Purkinje neurons after bone marrow transplant. Nat Cell Biol 5: 959–966.
17. Herzog EL, Van Arnam J, Hu B, Zhang J, Chen Q, et al. (2007) Lung-specific nuclear reprogramming is accompanied by heterokaryon formation and Y chromosome loss following bone marrow transplantation and secondary inflammation. FASEB J 21: 2592–2601.
18. Jang YY, Collector MI, Baylin SB, Diehl AM, Sharkis SJ (2004) Hematopoietic stem cells convert into liver cells within days without fusion. Nat Cell Biol 6: 532–539.
19. Harris RG, Herzog EL, Bruscia EM, Grove JE, Van Arnam JS, et al. (2004) Lack of a fusion requirement for development of bone marrow-derived epithelia. Science 305: 90–93.
20. Murry CE, Soonpaa MH, Reinecke H, Nakajima H, Nakajima HO, et al. (2004) Haematopoietic stem cells do not transdifferentiate into cardiac myocytes in myocardial infarcts. Nature 428: 664–668.
21. Balsam LB, Wagers AJ, Christensen JL, Kofidis T, Weissman IL, et al. (2004) Haematopoietic stem cells adopt mature haematopoietic fates in ischaemic myocardium. Nature 428: 668–673.
22. Conboy IM, Conboy MJ, Wagers AJ, Girma ER, Weissman IL, et al. (2005) Rejuvenation of aged progenitor cells by exposure to a young systemic environment. Nature 433: 760–764.
23. Ishikawa F, Yasukawa M, Lyons B, Yoshida S, Miyamoto T, et al. (2005) Development of functional human blood and immune systems in NOD/SCID/IL2 receptor {gamma} chain(null) mice. Blood 106: 1565–1573.
24. Pearson T, Shultz LD, Miller D, King M, Laning J, et al. (2008) Non-obese diabetic-recombination activating gene-1 (NOD-Rag1 null) interleukin (IL)-2 receptor common gamma chain (IL2 r gamma null) null mice: a radioresistant model for human lymphohaematopoietic engraftment. Clin Exp Immunol 154: 270–284.
25. Yamauchi T, Takenaka K, Urata S, Shima T, Kikushige Y, et al. (2013) Polymorphic Sirpa is the genetic determinant for NOD-based mouse lines to achieve efficient human cell engraftment. Blood 121: 1316–1325.
26. Bruneau BG (2002) Transcriptional regulation of vertebrate cardiac morphogenesis. Circ Res 90: 509–519.
27. Kucia M, Halasa M, Wysoczynski M, Baskiewicz-Masiuk M, Moldenhawer S, et al. (2007) Morphological and molecular characterization of novel population of CXCR4+ SSEA-4+ Oct-4+ very small embryonic-like cells purified from human cord blood- preliminary report. Leukemia 21: 297–303.
28. Neijssen J, Pang B, Neefjes J (2007) Gap junction-mediated intercellular communication in the immune system. Prog Biophys Mol Biol 94: 207–218.
29. Laflamme MA, Myerson D, Saffitz JE, Murry CE (2002) Evidence for cardiomyocyte repopulation by extracardiac progenitors in transplanted human hearts. Circ Res 90: 634–640.
30. Müller P, Pfeiffer P, Koglin J, Schäfers HJ, Seeland U, et al. (2002) Cardiomyocytes of noncardiac origin in myocardial biopsies of human transplanted hearts. Circulation 106: 31–35.
31. Camargo FD, Green R, Capetanaki Y, Jackson KA, Goodell MA (2003) Single hematopoietic stem cells generate skeletal muscle through myeloid intermediates. Nat Med 9: 1520–1527.
32. Doyonnas R, LaBarge MA, Sacco A, Charlton C, Blau HM (2004) Hematopoietic contribution to skeletal muscle regeneration by myelomonocytic precursors. Proc Natl Acad Sci U S A 101: 13507–13512.
33. Camargo FD, Finegold M, Goodell MA (2004) Hematopoietic myelomonocytic cells are the major source of hepatocyte fusion partners. J Clin Invest 113: 1266–1270.
34. Willenbring H, Bailey AS, Foster M, Akkari Y, Dorrell C, et al. (2004) Myelomonocytic cells are sufficient for therapeutic cell fusion in liver. Nat Med 10: 744–748.
35. Bailey AS, Willenbring H, Jiang S, Anderson DA, Schroeder DA, et al. (2006) Myeloid lineage progenitors give rise to vascular endothelium. Proc Natl Acad Sci U S A 103: 13156–13161.
36. Helming L, Gordon S (2007) The molecular basis of macrophage fusion. Immunobiology 212: 785–793.
37. Simmons PJ, Przepiorka D, Thomas ED, Torok-Storb B (1987) Host origin of marrow stromal cells following allogeneic bone marrow transplantation. Nature 328: 429–432.
38. Laver J, Jhanwar SC, O'Reilly RJ, Castro-Malaspina H (1987) Host origin of the human hematopoietic microenvironment following allogeneic bone marrow transplantation. Blood 70: 1966–1968.
39. Rose RA, Jiang H, Wang X, Helke S, Tsoporis JN, et al. (2008) Bone marrow-derived mesenchymal stromal cells express cardiac-specific markers, retain the stromal phenotype, and do not become functional cardiomyocytes in vitro. Stem Cells 26: 2884–2892.
40. Noiseux N, Gnecchi M, Lopez-Ilasaca M, Zhang L, Solomon SD, et al. (2006) Mesenchymal stem cells overexpressing Akt dramatically repair infarcted myocardium and improve cardiac function despite infrequent cellular fusion or differentiation. Mol Ther 14: 840–850.
41. Dayan V, Yannarelli G, Billia F, Filomeno P, Wang XH, et al. (2011) Mesenchymal stromal cells mediate a switch to alternatively activated monocytes/macrophages after acute myocardial infarction. Basic Res Cardiol 106: 1299–1310.

Acknowledgments

We thank H. Fujii for excellent technical support on histological analysis of recipient cardiac tissue; N. Aoki for excellent technical support on histological analysis of recipient bone; S. Yoshida and C. Iwamoto for helpful advice; N. Kinukawa for helpful comments on statistical analysis.

Author Contributions

Discussion: MH KA. Conceived and designed the experiments: MF FI MH KA. Performed the experiments: MF FI YN TY KM HS TK K. Nakamura. Analyzed the data: MF FI YN YS KT KS KO K. Nagafuji. Contributed reagents/materials/analysis tools: TK K. Nakamura. Wrote the paper: MF FI YN YS.

42. Ferreira-Martins J, Ogórek B, Cappetta D, Matsuda A, Signore S, et al. (2012) Cardiomyogenesis in the developing heart is regulated by c-kit-positive cardiac stem cells. Circ Res 110: 701–715.
43. Bu L, Jiang X, Martin-Puig S, Caron L, Zhu S, et al. (2009) Human ISL1 heart progenitors generate diverse multipotent cardiovascular cell lineages. Nature 460: 113–117.
44. Quaini F, Urbanek K, Beltrami AP, Finato N, Beltrami CA, et al. (2002) Chimerism of the transplanted heart. N Engl J Med 346: 5–15.
45. Genead R, Danielsson C, Andersson AB, Corbascio M, Franco-Cereceda A, et al. (2010) Islet-1 cells are cardiac progenitors present during the entire lifespan: from the embryonic stage to adulthood. Stem Cells Dev 19: 1601–1615.
46. Barile L, Cerisoli F, Frati G, Gaetani R, Chimenti I, et al. (2011) Bone marrow-derived cells can acquire cardiac stem cells properties in damaged heart. J Cell Mol Med 15: 63–71.
47. Kajstura J, Rota M, Whang B, Cascapera S, Hosoda T, et al. (2005) Bone marrow cells differentiate in cardiac cell lineages after infarction independently of cell fusion. Circ Res 96: 127–137.
48. Bergmann O, Bhardwaj RD, Bernard S, Zdunek S, Barnabé-Heider F, et al. (2009) Evidence for cardiomyocyte renewal in humans. Science 324: 98–102.
49. Metzele R, Alt C, Bai X, Yan Y, Zhang Z, et al. (2011) Human adipose tissue-derived stem cells exhibit proliferation potential and spontaneous rhythmic contraction after fusion with neonatal rat cardiomyocytes. FASEB J 25: 830–839.
50. Schmittgen TD, Livak KJ (2008) Analyzing real-time PCR data by the comparative C(T) method. Nat Protoc 3: 1101–1108.